การเพิ่มการละลายของพิโนสโทรบินโดยการสร้างสารประกอบเชิงซ้อน
กับบีตาไซโคลเดกซ์ทรินและอนุพันธ์

นางสาวจินตวีร์ กิขุนทด

วิทยานิพนธ์นี้เป็นส่วนหนึ่งของการศึกษาตามหลักสูตรปริญญาวิทยาศาสตรมหาบัณฑิต
สาขาวิชาชีวเคมีและชีววิทยาโมเลกุล ภาควิชาชีวเคมี
คณะวิทยาศาสตร์ จุฬาลงกรณ์มหาวิทยาลัย
ปีการศึกษา 2558

SOLUBILITY ENHANCEMENT OF PINOSTROBIN BY COMPLEXATION WITH β-CYCLODEXTRIN AND ITS DERIVATIVES

Miss Jintawee Kicuntod

A Thesis Submitted in Partial Fulfillment of the Requirements
for the Degree of Master of Science Program in Biochemistry and Molecular Biology
Department of Biochemistry
Faculty of Science
Chulalongkorn University
Academic Year 2015

Thesis Title	SOLUBILITY ENHANCEMENT OF PINOSTROBIN BY COMPLEXATIONWITH β-CYCLODEXTRIN AND ITS DERIVATIVES
By	Miss Jintawee Kicuntod
Field of Study	Biochemistry and Molecular Biology
Thesis Advisor	Dr.Thanyada Rungrotmongkol, Ph.D.
Thesis Co-Advisor	Professor Dr.Piamsook Pongsawasdi, Ph.D.

Accepted by the Faculty of Science, Chulalongkorn University in Partial Fulfillment of the Requirements for the Master's Degree

.... Dean of the Faculty of Science
(Associate Professor Dr.Polkit Sangvanich, Ph.D.)

THESIS COMMITTEE

.... Chairman
(Assistant Professor Dr.Kanoktip Packdibamrung, Ph.D.)

.... Thesis Advisor
(Dr.Thanyada Rungrotmongkol, Ph.D.)

.... Thesis Co-Advisor
(Professor Dr.Piamsook Pongsawasdi, Ph.D.)

.... Examiner
(Assistant Professor Dr.Kuakarun Krusong, Ph.D.)

.... External Examiner
(Associate Professor Dr.Siriporn Jungsuttiwong, Ph.D.)

จินตวีร์ กิขุนทด : การเพิ่มการละลายของพิโนสโทรบินโดยการสร้างสารประกอบเชิงซ้อนกับบีตาไซโคลเดกซ์ทรินและอนุพันธ์ (SOLUBILITY ENHANCEMENT OF PINOSTROBIN BY COMPLEXATIONWITH β-CYCLODEXTRIN AND ITS DERIVATIVES) อ.ที่ปรึกษาวิทยานิพนธ์หลัก: ดร.ธัญญดา รุ่งโรจน์มงคล, อ.ที่ปรึกษาวิทยานิพนธ์ร่วม: ศ. ดร.เปี่ยมสุข พงษ์สวัสดิ์, หน้า.

พิโนสโทรบินเป็นฟลาโวนอยด์ที่สำคัญชนิดหนึ่ง พบได้จำนวนมากในกระชาย และ ข่า คล้ายคลึงกับฟลาโวนอยด์ชนิดอื่นๆ พิโนสโทรบินมีความสามารถในการละลายน้ำต่ำ ซึ่งเป็นข้อจำกัดในการประยุกต์ใช้ทางด้านเภสัชกรรม บีตาไซโคลเดกซ์ทริน และ อนุพันธ์ ได้แก่ เฮปตะคิส-2,6-ได-ออโท-เมทิล-บีตาไซโคลเดกซ์ทริน (2,6-DMβCD) และ ไฮดรอกซีโพรพิลบีตาไซโคลเดกซ์ทริน (HPβCD) สามารถเพิ่มเสถียรภาพ และ การละลายน้ำของโมเลกุล guest ที่ละลายน้ำได้ต่ำ งานวิจัยนี้จึงมีเป้าหมายในการใช้วิธีการทางคอมพิวเตอร์ และ วิธีทางการทดลอง ศึกษาไดนามิกส์ และเสถียรภาพของพิโนสโทรบินซึ่งสร้างสารประกอบเชิงซ้อนกับบีตาไซโคลเดกซ์ทริน (βCD) และ อนุพันธ์ (2,6-DMβCD และ HPβCD) จากการศึกษาโมเลคิวลาร์ไดนามิกส์ซิมูเลชันพบว่า พิโนสโทรบินสามารถสร้างสารประกอบเชิงซ้อนกับบีตาไซโคลเดกซ์ทรินโดยทั้งวงแหวนโครโมน (*C*-PNS) และ วงแหวนฟีนิล (*P*-PNS) สามารถเข้าสู่โพรงของไซโคลเดกซ์ทริน จากการคำนวณค่าพลังงานการยึดจับ พบลำดับเสถียรภาพของสารประกอบเชิงซ้อนที่ต่างกันได้ดังนี้ 2,6-DMβCD > HPβCD > βCD ซึ่งสอดคล้องกับค่าคงที่เสถียรภาพจากวิธีทางการทดลอง แผนภาพเฟสการละลายชนิด A_L แสดงการเตรียมสารประกอบเชิงซ้อนแบบ 1:1 สารประกอบเชิงซ้อนที่แท้จริงได้จากการเตรียมแบบแช่เยือกแข็งซึ่งแสดงลักษณะโดยเทคนิคการเปลี่ยนแปลงความร้อน (DSC) และ แผนภาพสเปกตราของเอ็นเอ็มอาร์แบบสองมิติชนิด ROESY (2D-ROESY NMR) ผลจากสเตียร์โมเลคิวลาร์ไดนามิกส์ซิมูเลชัน และ 2D-ROESY พบว่า วงแหวนทั้งสองของพิโนสโทรบินสามารถเข้าสู่โพรงของอนุพันธ์บีตาไซโคลเดกซ์ทริน ขณะที่ วงแหวนโครโมน (*C*-PNS) ชอบเข้าสู่โพรงของบีตาไซโคลเดกซ์ทริน นอกจากนี้ยังพบว่าสารประกอบเชิงซ้อนของพิโนสโทรบินมีค่าการละลายสูงกว่าพิโนสโทรบินอิสระ เมื่อศึกษาผลทางชีวภาพพบว่าพิโนสโทรบินอิสระและสารประกอบเชิงซ้อนมีฤทธิ์ในการต้านการอักเสบเล็กน้อย ขณะที่มีฤทธิ์ในการต้านเซลล์มะเร็งปากมดลูกและมะเร็งเต้านมปานกลาง

ภาควิชา ชีวเคมี	ลายมือชื่อนิสิต ....
สาขาวิชา ชีวเคมีและชีววิทยาโมเลกุล	ลายมือชื่อ อ.ที่ปรึกษาหลัก ....
ปีการศึกษา 2558	ลายมือชื่อ อ.ที่ปรึกษาร่วม ....

5671924523 : MAJOR BIOCHEMISTRY AND MOLECULAR BIOLOGY
KEYWORDS: PINOSTROBIN / CYCLODEXTRIN / INCLUSION COMPLEX / MOLECULAR DYNAMICS SIMULATION / PHYSICAL AND BIOLOGICAL ACTIVITIES

JINTAWEE KICUNTOD: SOLUBILITY ENHANCEMENT OF PINOSTROBIN BY COMPLEXATIONWITH β-CYCLODEXTRIN AND ITS DERIVATIVES. ADVISOR: DR.THANYADA RUNGROTMONGKOL, Ph.D., CO-ADVISOR: PROF. DR.PIAMSOOK PONGSAWASDI, Ph.D., pp.

Pinostrobin (PNS) is one of the important flavonoids and can be abundantly found in the rhizomes of fingerroot *Boesenbergia rotrunda* and galangal *Alpinia galangal* and *A. officinarum*. Similar to other flavonoids, PNS has an extremely low water solubility that limits its use in pharmaceutical applications. Beta-cyclodextrin (βCD) and its derivatives, heptakis (2,6-di-*O*-methyl)-βCD (2,6-DMβCD) and 2-hydroxypropyl-βCD (HPβCD), can enhance the stability and solubility of low-soluble guest molecules. In the present work, computational and experimental studies were applied to investigate the dynamics and stability of PNS inclusion complexes with βCD and its derivatives, 2,6-DMβCD and HPβCD. From molecular dynamics (MD) study, PNS was able to form complexes with all βCDs by either the chromone (*C*-PNS) or phenyl (*P*-PNS) ring dipping towards the cavity. According to calculated binding free energies, the stability of the different PNS/βCDs complexes was in the order of 2,6-DMβCD > HPβCD > βCD in good agreement with the experimental stability constants. The A_L-type diagram exhibited the formed inclusion complexes with the 1:1 molar ratio. The inclusion complexes were successfully prepared by freeze-drying method and characterized by DSC and 2D-ROESY NMR techniques. Steered MD and 2D-ROESY results revealed the both binding modes of PNS favorably occupied inside the cavity of βCD derivatives, whilst *C*-PNS likely preferred to interact with the parental βCD. All PNS/βCDs complexes had a higher dissolution rate than the free PNS. Both PNS and its complexes significantly exerted a lowering effect on the IL-6 secretion in LPS-stimulated macrophages and showed a moderate cytotoxic effect against HeLa and MCF-7 cancer cell lines *in vitro*.

Department:	Biochemistry	Student's Signature	....
Field of Study:	Biochemistry and Molecular Biology	Advisor's Signature	....
		Co-Advisor's Signature	....
Academic Year:	2015		

ACKNOWLEDGEMENTS

This thesis is the resulting of my research in Master degree that had been spent for three years. There are many people who are always accompanied and supported me. First of all, I would like to express my deep gratitude to my advisor, Dr. Thanyada Rungrotmongkol, for her valuable guidance, cheerfulness, encouragement and kind understanding since I was studied in undergraduate throughout for years. It is not only the aspect of scientific work but I have also learned many great things from her such as her kind attitude, positive thinking and the best supporter. Because of her support, I had the great opportunities and gained many experiences to do scientific research on abroad. I wish to express my deeply appreciate to my co-advisor, Prof. Dr. Piamsook Pongsawasdi, for her valuable suggestion, comment, kind encouragement and understanding throughout this study. In addition, I would like to express my gratitude to Prof. Dr. Peter Wolschann who gave me the best occasion to do my thesis project at Department of Pharmaceutical Technology and Biopharmaceutics, University of Vienna, Austria for his excellent discussion. Also, I would like to thank MMag. DI. Dr. Monika Müller and Ms. Roswitha Schuster for their kindness, advice and dedicating their time for teaching and discussion. Moreover, I would like to special thank to Prof. Dr. Kato Koichi and Asst. Prof. Saeko Yanaka at Institute for Molecular Science and Okazaki Institute for Integrative Bioscience, Japan that accepted me to practice on protein work and allowed me to use high efficiency NMR spectroscopy and also sacrifice their valuable time to discuss and suggest me. Furthermore, I would like to express my billion thanks to Ms. Wasinee Khuntawee for her vauable time, suggestion, and kind. I would like to thank my friends, all member of Starch and Cyclodextrin Research Unit and members of Computational Chemistry Unit Cell (CCUC) for their welling helping and cheerfulness.

I would like to thank the scholarship from Graduate School, Chulalongkorn University to commemorate the 72nd anniversary of His Majesty King Bhumibol Adulyadej and the 90th Anniversary of CU Fund (Ratchadapiseksomphot Endowment Fund) to support my work. This research was also funded by the Ratchadapisek Sompoch Endowment Fund (2015), Chulalongkorn University (CU-58-013-FW). This work was supported in part by grants (25102001, 25102008 to K.K.) from the Ministry of Education, Culture, Sports, Science and Technology (MEXT) of Japan, and the Institute for Molecular Science International Internship Program in Asia (IMS-IIPA). The Computer Chemistry Unit Cell, and the Vienna Scientific Cluster (VSC-2) are acknowledged for facility and computing resources. Ultimately, I would like to express my deeply gratitude to my parents for their eternity love, understanding, cheerfulness and encouragement throughout my life and educations.

CONTENTS

Page

LIST OF TABLES

LIST OF FIGURES

Page

LIST OF ABBREVIATIONS

A_{290}	absorbance at 290 nm
βCD	beta-cyclodextrin
C_g	center of gravity
C-PNS	chromone ring of pinostrobin
^oC	degree Celsius
2,6-DMβCD	heptakis (2, 6-di-*O*-methyl) -beta-cyclodextrin
DMSO-d_6	dimethyl sulfoxide-d_6
D_2O	deuterium oxide
DSC	differential scanning calorimetry
ΔE_{ele}	electrostatic interaction energy
ΔE_{vdw}	van der Waals interaction energy
g	gram
ΔG_{bind}	Gibbs binding free energy
HPβCD	hydroxypropyl-beta-cyclodextrin
HPLC	high performance liquid chromatography
ΔH	entralpy
J	joule
K	kelvin
Kcal	kilocalories
K_c	stability constant
MD	molecular dynamics simulation
mg	milligram

ml	milliliter
mM	millimolar
MM/GBSA	the molecular mechanics-Generalized Born surface area
MM/PBSA	the molecular mechanics-Poissan-Boltzmann surface area
MTT	thiazolyl blue tetrazolium bromide
nm	nanometer
NMR	nuclear magnetic resonance
PES	potential energy surface
PNS	pinostrobin
P-PNS	phenyl ring of pinostrobin
RDF	radial distribution function
RMSD	root mean square displacement
S_0	intrinsic solubility
ΔS	entropy
SMD	steered molecular dynamic simulations
V	volum

CHAPTER I

INTRODUCTION

Nowadays, the herbal plants are widely growing up to apply in pharmaceutical field which are used as the functional food, dietary supplement and developed drugs since they are comprised of various secondary metabolites such as flavonoids, terpenoids, alkaloids, tannins and etc. [1]. Flavonoids are a large group of heterocyclic compounds that are commonly found in fruits, vegetables and herbs as plant secondary metabolites [2, 3]. A fairly diversified range of bioactivities, such as anti-bacterial, anti-allergic and anti-oxidative activities, have been reported for flavonoids [4, 5]. They are widely used as drug and dietary supplements due to their potential pharmacological properties and their rather low toxicity. Pinostrobin (PNS) is a kind of secondary metabolites belongs to the flavanone subclass of flavonoids (Fig. 1A) and can be extracted from the rhizomes of Thai galangal *Alpinia rotundra* and *A. officinarum* and Chinese ginger *Boesenbergia rotunda*. It has several important biological activities, such as an anti-inflammatory role on the cyclooxygenase activity [6], anti-aromatase activity [7] and inhibition of HIV-1 protease [8]. Furthermore, the activity of the β-amyloid peptide related to Alzheimer's disease can be inhibited by PNS through reducing the oxidative damage and calcium overload as well as suppressing the mitochondrial pathway that is involved in the cellular apoptosis [9]. Additionally, PNS has several important biological activities, such as an anti-viral role on inhibiting the herpes simplex virus-1 (HSV-1) replication [10], anti-mutagenic activity [11], decreased the mycelia growth rate of the fungus *Cytospora persoonii*

[12] and inhibiting the malarial activity [13]. Moreover, the essential biological activities of PNS have been reported and indicated that PNS has a major role in anti-ulcer activity that could be indirectly affected to anti-oxidant mechanism [14]. According to Wu and co-workers study, it was also suggested that PNS exhibited the anti-oxidant activity by determining with *in vitro* 2, 2-diphenyl-1-picrylhydrazyl (DPPH) scavenging assay [15]. Furthermore, PNS inhibited the inflammatory agents TNF-α (IC_{50} < 22 μM) and IL-1β (IC_{50} < 40 μM) activating by murine macrophages in Sprague Dawley rats [16]. PNS had an effect on inhibiting aromatase activity and decreased the growth of MCF-7 cells (human breast cancer cells) induced by dehydroepiandrosterone sulfate (DHEAS) and the estrogen receptor of 17β-estradiol (E_2) [17]. Cao and co-workers study revealed that PNS could demonstrate the anti-tumor activity against HeLa and HepG2 cell lines [18]. Interestingly, the toxic effect on Wistar rats was evaluated at high dose of PNS and the result was found that LD_{50} of PNS was more than 500 mg/kg. It can be described that PNS had non-toxic and non-genotoxic effects [19]. Similar to many flavonoids, PNS exhibits a relatively low water solubility leading to a significant limitation in its use in pharmaceutical applications. Consequently, suitable drug delivery carriers are of interest to solve this problem.

Cyclodextrins (CDs) are macrocyclic oligosaccharides of α-1,4 linked D-(+)-glucopyranose produced from starch by cyclodextrin glycosyl transferase catalysis [20]. CD structures have a truncated cone shape with a relatively hydrophilic outer surface and a hydrophobic inner cavity. The wider rim of CD consists of hydroxyl groups at the 2- and 3-position of each glucose subunit, while the other narrower rim contains hydroxyl groups at the 6-position of each glucose subunit.

The inclusion of poorly water-soluble drugs into CD can be used to enhance the solubility, stability and bioavailability of these drugs [21-23], where the hydrophobic drugs prefer to insert their hydrophobic motif(s) inside the CD cavity [24]. Naturally, there are three major types of small-ring CDs; namely αCD, βCD (Fig. 1B) and γCD that are composed of six, seven and eight glucose subunits, respectively [25]. Due to the high yield synthesis and low price of βCD, it has been the main form used in the pharmaceutical, food and cosmetic industries [26]. Besides, βCD can form host-guest inclusion complex with various inorganic/organic molecules and also natural drugs that can significantly increase their properties [27-29]. Albeit, βCD shows a relatively lower water solubility (18.5 mg/mL) than other CDs [30, 31], which limits its applications. Derivatives of βCD, for example 2,6-dimethyl βCD (2,6-DMβCD) and 2-hydroxypropyl βCD (HPβCD) that have a higher water solubility (570 and >600 mg/mL, respectively) [32, 33], have been shown to improve the bioavailability and bioactivity of the encapsulated molecule in a much more efficient way [34-36].

Experimental studies to determine the stability and phase solubility of inclusion complexes between CDs and flavonoids have been reported [37, 38], and have shown that a higher solubility of the CD derivatives and better affinities between host and guest molecules are advantages for pharmaceutical applications [39]. In recent study, the poor water soluble and the dissolution of herbal drugs are mainly challenge for formation of host-guest inclusion complex to improve their properties. The experimental studies on forming inclusion complex with derivatives of βCD showed higher solubility and bioavailability than complex with parental βCD. The formed inclusion complex of guest molecules that insert in cavity of βCDs can be characterized by various techniques e.g. Differential Scanning Calorimetry (DSC) and Nuclear Magnetic Resonance (NMR) spectroscopy [40-42]. For example, phase solubility studies on rutin forming 1:1 molar ratio complexes with HPαCD, HPβCD and HPγCD revealed that the complex stability constants with HPβCD and HPγCD were significantly increased [43]. Accordingly, the solubility of artesunate, a low water soluble antimalarial drug, can be improved by a 1:1 molar ratio formation with methyl-βCD better than with HPβCD or βCD. Also, the study on aqueous solubility and bioactivity of apigenin forming 1:1 molar ratio with several derivatives of βCD revealed that the solubility and anti-oxidant activity were significantly increased [44]. Furthermore, albendazole, a drug for gastrointestinal helminthic infection treatment, formed an inclusion complex with βCD derivatives (βCD, Hydroxypropyl-βCD, methyl- βCD and synthesized βCD-citrate derivative) in a 1:1 ratio. Albendazole complex with βCD derivatives showed a higher solubility and dissolution. Moreover, NMR spectroscopy and DSC data were also obtained to characterize the geometry of Albendazole molecule in cavity of βCDs [45].

In addition to experimental investigations, computational tools are useful to determine the preferable binding mode of drugs, such as flavonoids, and for the prediction of guest-host interactions as well as the stability of inclusion complexes at a molecular level [46]. For example, the molecular dynamics simulations (MDs) of quercetin and myricetin complexed with different CD derivatives provided the host-guest orientation in a good agreement with the ^{1}H-NMR results [47]. In addition, although there are various possible inclusion geometries of fisetin/βCD complexes, it was found by molecular simulations that the insertion of the phenyl ring inside the cavity of βCD was more favorable [48]. Moreover, the molecular mechanics-Poissan-

Boltzmann surface area/-generalized Born surface area (MM-PBSA/GBSA) and quantum mechanics (QM)-PBSA/GBSA binding free energy calculations predicted that naringenin would bind to 2,6-DMβCD better than to natural βCD [49]. Furthermore, the steered molecular dynamics (SMD) simulation was introduced to understand of the binding process between βCD and four guest molecules (puerarin, daidzin, daidzein and nabumetone). The results showed asymmetric free energy profiles of each guest molecule arrangement and it can be indicated that guest molecules had two types of inclusion complexes [50].

To date, theoretical and experimental studies of PNS in inclusion complexes with various βCDs have not been reported. Thus, the main aim of this study was to predict computationally the most suitable βCD derivative for PNS encapsulation, and then the PNS/βCD complexes were formed experimentally for further pharmaceutical applications. The effect of temperature on solubility of PNS and the stoichiometry of guest-host complex by employing phase solubility study were also studied in this work. The inclusion complexes were characterized for their physical properties by Differential Scanning Calorimetry (DSC) and two-dimensional ^{1}H rotational frame Overhauser effect spectroscopy (2D ROESY NMR). Furthermore, dissolution and biological activities of inclusion complexes were evaluated and compared to free compound of PNS. In addition, the molecular details of the PNS binding mode and orientation, stability and solvation in the inclusion complexes with βCD and its derivatives, 2,6-DMβCD and the three HPβCDs (2- and 6-HPβCD and 2,6-DHPβCD), were discussed and compared by the molecular dynamics (MD) simulation and the steered molecular dynamics (SMD) simulation techniques.

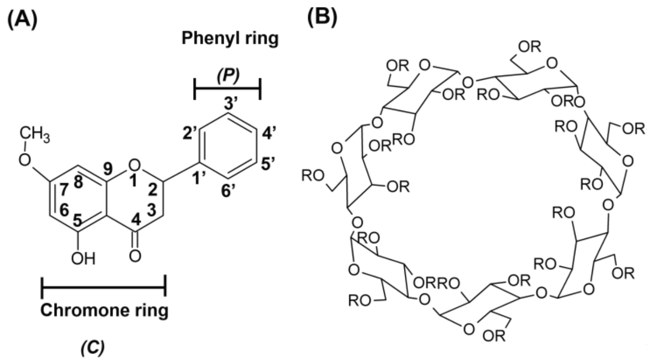

Fig. 1 Two dimensional structures of (A) pinostrobin (PNS) and (B) β-cyclodextrin (βCD) and its derivatives used in the present study, where –R is –H, $–CH_3$ and $–C_3H_7O$ for βCD, 2,6-DMβCD and 2,6-DHPβCD, respectively.

CHAPTER II

MATERIALS AND METHODS

2.1 Equipment

Accelrys Discovery Studio 2.5	: Biovia, USA
AMBER 12 molecular dynamic package	: University of California, USA
Analytical balance	: Mettler Toledo, Switzerland
Centrifuge	: Centrifuge 5430 R, eppendorf, Germany
High Performance liquid chromatography	: SCL-10A VP, Shimazu, Japan
HPLC Column, 150x10 mm I.D.	: Hydrosphere C18, YMC America Inc., USA
Lyophilizer	: LYO-LAB, Lyophilization Systems Inc., USA
Microplate reader	: Genios Pro microplate reader, Tecan, Crailsheim, Germany
Nuclear Magnetic Resonance Spectrometer	: Bruker 500 Ultrasheild, UK
Nylon Syringe Filter	: Merck Millipore Ltd., Ireland
Shaker water bath	: Memmert, Germany
Syringe	: Terumo, Japan
The GROMACS package	: version 4.6.5
Thermal analyzer (DSC)	: 822e apparatus, Mettler Toledo, USA

UV-Vis Spectrophotometer	: DU 800 Spectrophotometer, Beckman Coulter, USA
Vortex	: Model G-560E, Scientific Industries, USA

2.2 Chemicals

Anti-Mouse IL-6	: eBioscience Inc., San Diego, USA
β-cyclodextrin, MW=1135 g/mol	: HPLC grade, Wako Pure Chemical industries, Japan
Breast cancer (MCF-7) cells	: The American Type Cell Culture Collection (ATCC), USA
Compounds for phosphate buffer saline (PBS)	: Sigma-Aldrich, Darmstadt, Germany
Deuterium oxide (D_2O)	: Cambridge Isotope Laboratories Inc., USA
Dimethyl sulfoxide-d_6 (DMSO-d_6)	: D034, Euriso-top, USA
Dulbecco's Modified Eagle's medium (DMEM)	: Life Technologies, Carlsbad, CA, USA
Heptakis (2, 6-di-*O*-methyl) -β-cyclodextrin, MW= 1331.36 g/mol	: H0513-5G, Sigma-Aldrich, Singapore

Human cervical carcinoma (HeLa) cells	: The American Type Cell Culture Collection (ATCC), USA
Human colon cancer (Caco-2) cells	: The American Type Cell Culture Collection (ATCC), USA
(2-Hydroxypropyl) -β-cyclodextrin , MW= 1396 g/mol, DS = 0.5-1.3	: H107-5G, Sigma, Singapore
Lipopolysaccharides (LPS) from *Escherichia coli* O111:B4	: Sigma-Aldrich, Darmstadt, Germany
Methanol	: 99.8% (mass/mass), Wako, Japan
Milli Q water	: Millipore, France
Pinostrobin	: Extracted from rhizomes of Fingerroot (*Boesenbergia rotrunda*)
Sodium Dodecyl Sulfate (SDS)	: Sigma-Aldrich, Darmstadt, Germany
The murine macrophage cell lines (RAW 264.7)	: The American Type Cell Culture Collection (ATCC), USA
Thiazolyl blue tetrazolium bromide (MTT)	: Sigma-Aldrich, Darmstadt, Germany

Trifluoro acetic acid (TFA) : 1 ml x 5, Nacalai lesque, Kyoto, Japan

2.3 Molecular dynamics (MD) simulation method

2.3.1 System preparation

The optimized structures of βCD and 2,6-DMβCD were taken from our previous studies [51]. For the three HPβCD derivatives, the structures of 2-HPβCD, 6-HPβCD and 2,6-DHPβCD were prepared by 2-hydroxylpropyl substitutions on all 2-, 6- and both 2- and 6-hydroxyl positions of the natural βCD, respectively. The PNS geometry was built and then optimized by the HF/6-31(d) level of theory using the Gaussian09 program to obtain well-adjusted bond lengths and angles [52]. The inclusion complex between PNS and each respective (modified or not) βCD was constructed by the CDOCKER module in the Discovery Studio 2.5 (Accelrys, Inc.) with 500 independent docking runs. The complex with the best ranked interaction energy and highest hydrogen bond (H-bond) formation at each PNS binding mode, chromone (*C*-PNS) or phenyl ring (*P*-PNS) dipping into the βCD cavity, was chosen as the representative structure. Where only one binding orientation was obtained by the docking procedure, another was manually generated for comparison. In total, there were 15 systems for further MD studies; five free CDs (βCD, 2,6-DMβCD, 2,6-DHPβCD, 2-HPβCD and 6-HPβCD) plus these five different CDs complexed with either *P*-PNS or *C*-PNS. Note that the docking manner was used to determine the starting position of PNS in βCDs. Hence, the molecular dynamics (MD) simulation was performed to clarify the importance of solvent effects in the forming inclusion complexes.

2.3.2 Molecular dynamics (MD) simulation

The structure of βCD and its dimethyl and hydroxypropyl derivatives alone and complexed with PNS in aqueous solution were simulated with three different initial velocities using the Amber 12 software package [53]. The parameters of βCD and its derivatives were taken from the Glycam06 carbohydrate force field [54], while the partial charges and empirical parameters of PNS were obtained by the standard procedures described elsewhere [55-59]. To relax the structure prior to simulation, the hydrogen atoms of each system were minimized with 1000 steps of steepest descents (SD) and continued by 3000 steps of conjugated gradient (CG). The simple point charge (SPC) water molecules were then used to solvate around the inclusion complexes with the minimum distance of 12 Å from the system surface. As a result, the truncated octahedron periodic water box size of the simulated systems was approximately 45 x 45 x 45 $Å^3$ and consisted of 1400±42 water molecules. The SD (1000 steps) and CG (3000 steps) minimizing procedure was applied to the whole system. The periodic boundary condition with *NPT* ensemble was applied for all simulations. The cutoff distance for electrostatic interactions was set at 12Å according to the particle mesh Ewald approach [60]. To constrain all bonds involving hydrogen atoms, the SHAKE algorithm was used. The systems were heated up to 298 K for 100 ps, and then were continuously held at constant temperature of 289 K for 80 ns. The integration time was set at 2 fs and the MD trajectories were collected every 2 ps. The equilibrium state of simulated systems was considered by the root mean square displacement (RMSD). The conformation changes in βCD and its derivatives in the free form and when complexed with PNS were discussed in terms of the potential energy surface (PES). The mobility and water accessibility of PNS in the cavity of βCD and each derivative were determined by measurement of the distances between PNS and the respective βCD or derivative molecule and the radial distribution functions (RDF) of water around the PNS hetero atoms, respectively. Using the same trend of binding free energy prediction reported previously using the MM- and QM-PBSA/GBSA methods in the flavonoid/CD complexes [48, 49], the MM-GBSA approach was adopted to estimate the binding affinity of PNS and βCDs in this study. All structural data were analyzed by the ptraj module, while the binding free energy was calculated by MM-GBSA module implemented in Amber program.

2.3.2.1 MM-GBSA calculation

The MM-GBSA is acceptable method in Amber package to evaluate the free energies of binding or to estimate the absolute free energies of molecules in solution. The binding free energy of system was obtained from the difference of the free energies between complex (ΔG_{cpx}), β-Cyclodextrin ($\Delta G_{\beta\text{-}CD}$) and ligand ($\Delta G_{lig}$) as shown by:

$$\Delta G_{\mathrm{bind}} = \Delta G_{cpx} - [\Delta G_{\beta\text{-}CD} + \Delta G_{lig}] \qquad (1)$$

In general, the total free energy computes from the enthalpy term (ΔH) and entropic contribution at a constant temperature $(T\Delta S)$.

$$\Delta G = \Delta H - T\Delta S \qquad (2)$$

The ΔH term of the system was obtained the summation of enthalpy changes in the gas phases upon complex formation (ΔE_{MM}) and the solvated free energy contribution (ΔG_{sol}). From Eq. (2) can be approximated as:

$$\Delta G = (\Delta E_{MM} + \Delta G_{sol}) - T\Delta S \qquad (3)$$

Where ΔE_{MM} corresponds to the molecular mechanical energy, including the bonded and non-bonded energy terms. The latter one is composed of the electrostatic (ΔE^{ele}) and vdW (ΔE^{vdw}) interaction energies. ΔG_{sol} accounts for the solvation energy which is divided into the electrostatic component (ΔG_{sol}^{ele}) and a nonpolar component $(\Delta G_{sol}^{nonpolar})$.

$$\Delta G_{sol} = \Delta G_{sol}^{ele} + \Delta G_{sol}^{nonpolar} \tag{4}$$

The non-polar term is assumed to the surface accessible surface area (SASA) in Eq. (5). The polar term is calculated from the Poisson Boltzmann (PB) equation in Eq. (6) or the generalized Born (GB) in Eq. (7). The increasing in SASA is associated with an increase in solvation free energy, which is partly calculated for non-polar and excluded in term of solvent, using Eq. (8). The solvation parameters, γ and β, depend on the method and solvation models.

$$\Delta G_{sol} = \Delta G_{PB(GB)} + \Delta G_{SASA} \tag{5}$$

$$\Delta G_{PB} = \frac{1}{2}\sum_{qi}(\varphi_i^{80} - \varphi_i^{1}) + \Delta G_{SASA} \tag{6}$$

$$\Delta G_{GB} = -166(1-\frac{1}{e})\sum_{i=1}^{n}\sum_{j=1}^{n}\frac{q_i q_j}{fm2GB} + \Delta G_{SASA} \tag{7}$$

$$\Delta G_{SASA} = \gamma SASA + \beta \tag{8}$$

2.4 Steered molecular dynamics (SMD) simulation method

The Amber Glycam06 carbohydrate FF and GAFF parameters applied for CDs and PNS, respectively, were converted to a proper format for GROMACS by AnteChamber PYthon Parser interfacE (ACPYPE) [61]. All steered molecular dynamics simulations were performed by GROMACS package (version 4.6.5). Each system contained an inclusion complex surrounded with approximately 3200 SPC water molecules in a cubic box of 4.5 x 4.5 x 4.5 nm^3. The PNS was then set at the center of the box with the Z-coordinate of cyclodextrin that was approximately located at Z equal to 2 nm. To equilibrate the simulated system prior to production, the whole system was minimized with 50000 steps of steepest descents (SD) and continued by 20000 steps of conjugated gradient (CG). Under periodic boundary condition with *NPT* ensemble, the system was heated at constant temperature of 289 K for 1 ns. The particle mesh Eward (PME) approach was used to treat long-range electrostatic interactions with non-bonded cut-off of 1 nm. The core CD was restrained and used as an immobile reference for ligand pulling. PNS was pulled out through the lipophilic cavity from secondary rim (wider rim) along the Z-axis with a harmonic force constant of 2000 kJ mol^{-1} nm^{-1} and a pulling rate of 0.0010 nm ps^{-1} for approximately 2 ns.

2.5 Experimental methods

2.5.1 Analysis of Pinostrobin

2.5.1.1 Spectrophotometric method

2.5.1.1.1 The maximum absorption of Pinostrobin

The UV absorption spectrum for free compound of PNS, three β-cyclodextrins (βCD, 2,6-DMβCD and HPβCD) and the three inclusion complexes (PNS/βCD, PNS/2,6-DMβCD and PNS/HPβCD) were prepared by dissolving equivalent amount of free compounds and the inclusion complexes in 10 ml of deionized water. Then, absorption spectra were measured in the wavelength range of 200-400 nm.

2.5.1.1.2 Standard curve of Pinostrobin

2.7 mg of PNS was accurately weighed and dissolved in 50 ml of deionized water. This solution was boiled at 60 °C for an hour and used as stock solution of PNS (~ 0.19 mM). Then, the standard solutions were prepared by serial diluting the stock solution to the final concentrations of 0 to 0.1 mM (0, 0.01, 0.02, 0.04, 0.06, 0.08 and 0.1 mM). All standard solutions were analyzed for the absorbance at λ_{max} obtained from 2.5.1.1.1. The standard curve was then plotted.

2.5.1.2 High Performance liquid chromatography method

2.5.1.2.1 Standard curve of Pinostrobin

The free compound of PNS was accurately weighed (2.7 mg) and dissolved in Milli Q water 50 ml. This solution was overnight incubated at 37 °C and used as stock solution of PNS (~ 0.19 mM). The stock solution was filtered with 0.45 µm Nylon membrane and standard solutions were prepared by serial dilution the stock solution to the final concentrations of 0 to 0.15 mM. All standard solutions were analyzed the absorbance at 290 nm by HPLC on a C18 reverse phase column, elution was by 70:30 MeOH:Milli Q water. The standard curve was then plotted.

2.5.2 Phase-solubility diagram

An excess amount of PNS was dissolved in 0-10 mM βCD, 2,6-DMβCD and HPβCD, respectively. The mixtures were shaken in a water bath at 16, 25, 30, 37 and 45 °C, respectively for 72 hours. The dissolved PNS concentration at each temperature was determined by UV-Vis spectrophotometer at 290 nm which is the maximum wavelength of PNS. Each experiment was performed in triplicate. Furthermore, the solubility of PNS in deionized water was also determined in the same manner. The phase solubility diagrams of PNS in the presence of various concentrations of βCD and its derivatives were obtained using the method of Higuchi and Connors [62]. The stability constant (K_C) of PNS when dissolved in different βCDs at various temperatures were calculated from the slope data of the phase solubility linear diagrams according to Eq. (9)

$$K_C = \frac{Slope}{S_0(1 - Slope)} \tag{9}$$

where S_0 is the saturation concentration of PNS in water at each temperature.

2.5.3 Preparation of the solid inclusion complexes

Two methods were used for preparation of the solid complexes. These included physical mixing and freeze-drying methods. The mole ratio of PNS and βCDs were prepared as 1:1.

2.5.3.1 Physical mixing method

PNS, βCD and its derivatives were accurately weighed as equivalent amount. Afterwards, PNS and each βCD were physically mixed at room temperature. Then, all of mixing powders were used as control and kept in a desiccator for further analysis.

2.5.3.2 Freeze drying method

PNS and each βCD were accurately weighed, and dissolved in 30 ml of deionized water. The solutions were magnetic stirred until they were completely dissolved. The solutions should be warmed at room temperature before freeze at -80 °C overnight and subjected to the lyophilizer (LYO-LAB, Lyophilization Systems) for 2 days. The freeze-dried powder products were kept in a desiccator for further analysis.

2.5.4 Characterization of inclusion complexes

2.5.4.1 Differential Scanning Calorimetric analysis (DSC)

DSC thermograms were obtained from DSC 822e apparatus (Mettler Toledo, USA). All solid complexes were characterized using 0.7-2.0 mg of samples in aluminium pans and heated at 10^{o}C/min in the temperature range of 50 to 300 ^{o}C.

2.5.4.2 Two-dimensional Nuclear Magnetic Resonance (ROESY-NMR)

2.5.4.2.1 Sample preparation

The three solid inclusion complexes (PNS/βCD, PNS/2,6-DMβCD and PNS/HPβCD) should be dissolved in the suitable solvents for getting the proper intensity of NMR signal. Since PNS/βCD complex was lower soluble than other complexes, it was then dissolved in 25:75 DMSO-d_6:D_2O whilst PNS/2,6-DMβCD and PNS/HPβCD were dissolved in 99.8% D_2O.

2.5.4.2.2 Measurements

Two-dimensional ROESY spectra of all inclusion complexes were measured by using AVANCE-500 spectrometer equipped with a 5 mm triple-resonance cryogenic probe (Bruker Biospin). The NMR data were processed and analyzed using TopSpin (Bruker BioSpin) software [63, 64].

2.5.5 Analysis of the inclusion complexes dissolution diagram

The equivalent amount of free compound (PNS) and freeze-dried complexes were accurately weighed, and dissolved in 20 ml of milli Q water. Then the solutions were shaken at 37 ^{o}C, 100 rpm for 4 hours. At the same time, 1 ml of each solution was withdrawn at different time intervals (0, 5, 10, 15, 20, 30, 40, 60, 120, 180 and 240 minutes). Each sample was filtered with 0.45 µm Nylon membrane. C 18 column was used to analyze the concentrations of dissolved PNS at 290 nm by HPLC. The HPLC mobile phase was consisting of 70:30 MeOH : Milli Q water.

2.5.6 Determination of biological activity of the inclusion complexes

2.5.6.1 Preparation of solutions

Four solutions were prepared and used as stock solutions for anti-inflammatory and cytotoxicity assays: they were free compound of PNS and its three inclusion complexes (PNS/βCD, PNS/2,6-DMβCD and PNS/HPβCD). To prepare 0.1 µM as a final concentration of stock solution, free compound of PNS and its complexes were dissolved in absolute EtOH and distilled water, respectively.

2.5.6.2 Anti-inflammatory assay

The murine macrophage cell line, RAW 264.7, was used to investigate the anti-inflammatory effect of the free compound and its inclusion complexes as previously described [65, 66]. Cells at a density of 2×10^6 per well in DMEM medium were cultured in 24 well plates and incubated at 37 °C for 24 hours. All stock solutions were diluted to the final concentrations of 10^{-1} to $2x10^{-4}$ µM. The diluted solutions were added to the cultured cells and pre-incubated for 3 hours before adding lipopolysaccharide (LPS) to the final concentration of 1µg/ml. After incubation of the cells at 37 °C for 24 hours, the supernatant was used for Enzyme Linked Immuno Sorbent Assay (ELISA) to determine the concentration of secreted IL-6. The ELISA was examined at room temperature following the manufacturer's procedure (eBiosciences, Santa Clara, CA, USA). The optical density was measured at 450 nm using an Infinite M200 microplate reader (Tecan, Crailsheim, Germany) which was corrected by the reference wavelength of 570 nm. Moreover, the cells that attached on the bottom of the wells were incubated with the MTT (thiazolyl blue tetrazolium bromide, Sigma-Aldrich (St. Louis, MO, USA; 0.5 mg/ml) for 3 hours at 37 °C. After that, cells were lysed with a buffer containing 10% SDS in 0.01 N HCl and the produced formazan (by viable cells) was measured at 570 nm and corrected by the reference wavelength at 690 nm. Note that the untreated and treated LPS cells acted as the negative and positive controls, respectively. The positive control was defined as 100% cytokine secretion. All experiments were performed in triplicates. The percentage of IL-6 secretion or cell viability was plotted against the concentrations of sample. The results are shown in Fig. 2. After that, the half maximum inhibitory concentration (IC_{50}) was calculated by Eq. (10) in Table Curve 2D (Systat Software, San Jose, CA, USA) [67].

$$Y = a + \frac{b}{1 + \left(\frac{c^d}{X} \right)} \tag{10}$$

where *a* represents the minimum of the curve, *b* is the difference between the curve maximum and minimum, *c* is the transition center of the curve which is the concentration that causes 50% reduction of cytokine secretion or cytotoxic and *d* is slope of the curve.

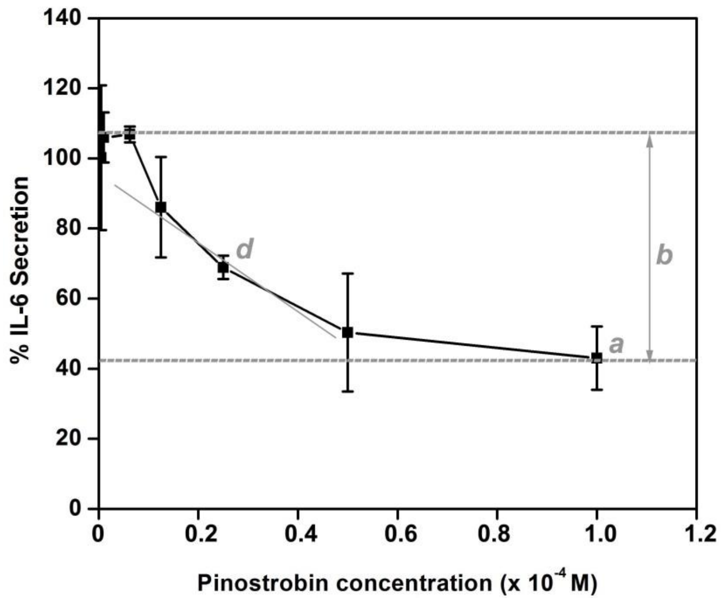

Fig. 2 The plot between the percentages of IL-6 secretion against the various concentrations of free PNS used for IC_{50} determination

2.5.6.3 Cytotoxicity assay

MTT assay based on the conversion of MTT by mitochondrial dehydrogenase of viable cells to formazan was used to determine the cell viability of three different cancer cell lines (the cervix carcinoma cell line HeLa and the breast cancer cell line MCF-7) treated with free PNS and its inclusion complexes. Thus the cytotoxicity of the samples against the cancer cell lines was derived. Briefly, cells at a density of $2x10^6$ were seeded into each well of 96-well plates and incubated at 37 °C for 24 hours. The cells were subsequently incubated for further 24 hours with the compound solutions. Then cells were incubated with MTT (0.5 mg/ml) for 2 hours. Afterwards, lysis buffer was added to lyse the cells. The formazan was measured at 570 nm with a reference wavelength of 690 nm. The positive control was the cells only incubated with DMEM and defined as 100% of the amount of cells. All experiments were performed in triplicates. The half maximum inhibitory concentration (IC_{50}) of the cytotoxic effect was determined using Table Curve 2D which was calculated by the same procedure of anti-inflammatory assay.

CHAPTER III

RESULTS AND DISCUSSIONS

3.1 Computations

3.1.1 Molecular dynamics (MD) simulation

The three independent simulations on each system provided relatively similar results. Thus, for simplification the data from only one simulation are presented here.

3.1.1.1 System stability

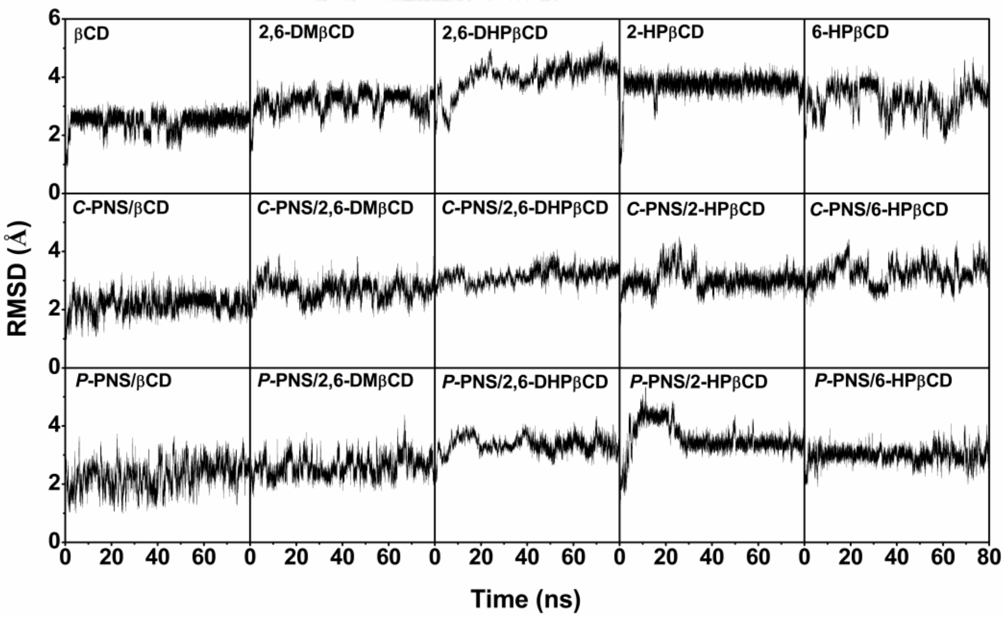

Fig. 3 RMSD plots of all atoms for the 15 simulated systems (βCD and its four derivatives alone and each complexed with either *C*-PNS or *P*-PNS) versus the simulation time.

To monitor the system stability, the RMSD with respect to the initial structure of the free CDs (βCD, 2,6-DMβCD and the three HPβCDs), and their complexes with PNS (as *C*-PNS and *P*-PNS) was calculated. The results are illustrated in Fig. 3, where, as expected, the averaged RMSD of the parent βCD was smaller than those of all the modified βCDs. Among the uncomplexed CDs, a noticeable fluctuation in the RMSD was observed in 6-HPβCD, which contains the hydroxypropyl substitutions at the 6-position, as found previously [70]. Complexation with PNS (both *P*-PNS and *C*-PNS conformations) led to a reduction in the RMSD values in all inclusion complexes. For instance, the RMSD of the *C*-PNS and *P*-PNS in complex with 2,6-DHPβCD was observed in a range of 3.0–3.5 Å, whilst the RMSD of the free 2,6-DHPβCD was larger than 4 Å. The differences in the RMSD fluctuations between the two relative complexes resulted from the structural and dynamic properties of PNS binding inside the host cavity (discussed later in Fig. 5). From the RMSD plots, it seems that all the simulated systems had reached equilibrium by 40 ns (except for the free 6-HPβCD), and so for each system the MDs trajectories from the 60 ns were extracted for further analysis.

3.1.1.2 Conformation of βCDs in free and complex forms

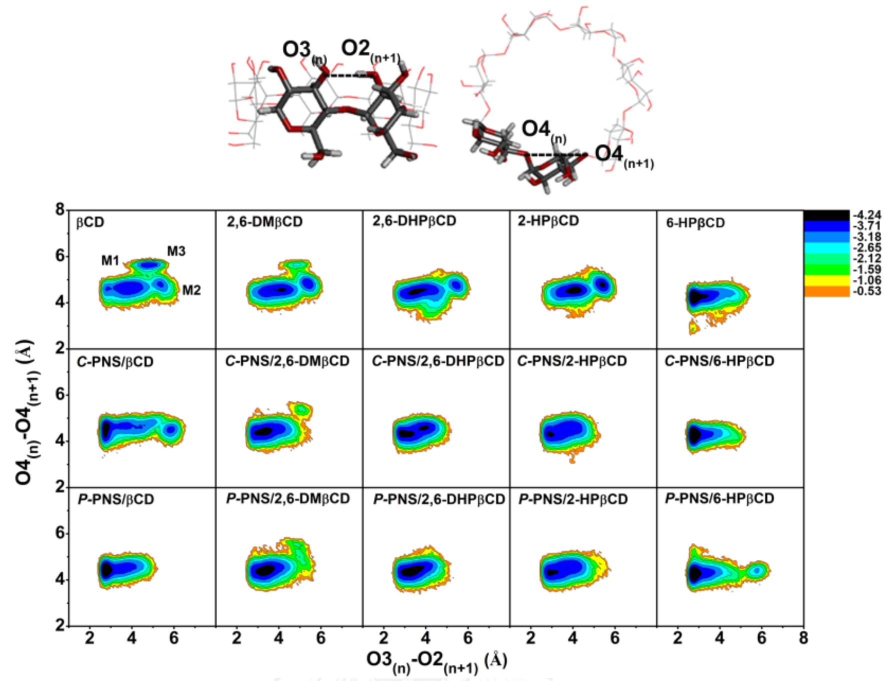

Fig. 4 The potential energy surface (PES) plots of the distance between the adjacent glycosidic oxygens, $O4_{(n)}$-$O4_{(n+1)}$, versus the intramolecular hydrogen bond distance, $O3_{(n)}$-$O2_{(n+1)}$, for the different βCDs (top row) alone or complexed with (middle row) *C*-PNS or (bottom row) *P*-PNS.

As seen from the RMSD plots, PNS might affect the conformation of the host βCDs molecule. To investigate such conformational changes, the distance between the glycosidic oxygen atoms ($O4_{(n)}$-$O4_{(n+1)}$) and the distances between the hydroxyl groups on the secondary rim of neighboring glucoses ($O3_{(n)}$-$O2_{(n+1)}$) were monitored from the last 40-ns snapshots. It has to be noticed that the second distance related to intramolecular hydrogen bond formation refers to the structural characteristic feature of CDs [68]. Using Eq. (11), the distributions of these two distances were calculated and are presented in terms of free energy in Fig. 4.

$$F(x,y) = -k_B T \log[P(x,y)] \tag{11}$$

where k_B is the Boltzmann constant and T is the absolute temperature. $P(x,y)$ is the probability of the parameters *distance* $(O3_{(n)}\text{-}O2_{(n+1)})$ and distance $(O4_{(n)}\text{-}O4_{(n+1)})$ as x and y, respectively.

In Fig. 4, the three minima M1, M2 and M3 were detected from the PES of parent βCD, with a free energy ranked in the order of M1 < M2 < M3. For the most probable conformation of βCD (M1), the $O3_{(n)}$-$O2_{(n+1)}$ distance was distributed in range of 3-5 Å with a possible formation of intramolecular hydrogen bonds on the wider rim (≤ 3.5 Å), while the $O4_{(n)}$-$O4_{(n+1)}$ distance was likely presented at ~4.5 Å. At the same $O4_{(n)}$-$O4_{(n+1)}$ distance, an outspread of the $O3_{(n)}$-$O2_{(n+1)}$ distance was found for M2. In contrast, the $O4_{(n)}$-$O4_{(n+1)}$ distance for M3 was lengthened over 5 Å and the $O3_{(n)}$-$O2_{(n+1)}$ distance was in between those of M1 and M2. Amongst all βCD derivatives in free form, only 2,6-DMβCD shared a similar PES to the unmodified βCD, while the M3 had totally disappeared within the others. Upon complexation with PNS the binding of PNS forced the βCDs structure to adopt the most stable conformation (a more dominant M1) with stronger intramolecular hydrogen bonds (higher proportion of $O3_{(n)}$-$O2_{(n+1)}$ with a distance ≤ 3.5 Å). In addition, the shape of βCDs also depended on the PNS binding mode, in particular for βCD and 6-HPβCD. Both M1 and M2 were detected in *C*-PNS/βCD and *P*-PNS/6-HPβCD complexes, whereas in the other cases only an M1 conformation was observed.

3.1.1.3 PNS mobility and preferential displacement in CD cavity

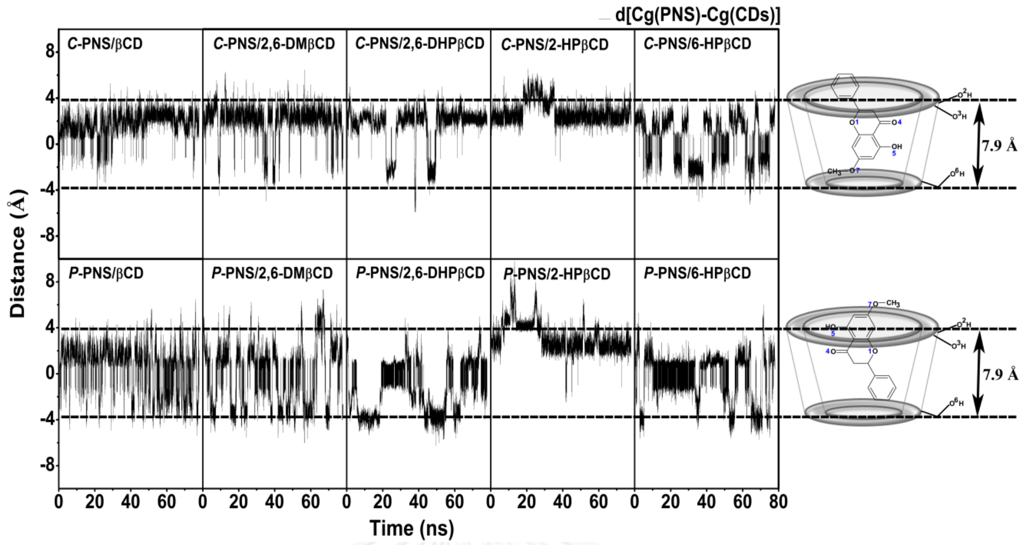

Fig. 5 Distance between the centers of gravity of PNS and CD excluding the modified functional groups for all systems. Dashed lines represent the cavity height of regular βCD.

The dynamic behavior of the *C*-PNS- or *P*-PNS binding towards the five different βCDs were determined by monitoring the distance from the center of gravity of PNS molecule to the center of gravity of each different CD without considering the functional modifications of the respective modified βCD molecule. The results of the 10 inclusion complexes were plotted and compared in Fig. 5, where the horizontal dashed lines at -3.95 Å and 3.95 Å represent the positions of the primary and secondary rims of βCD, respectively [29]. It can clearly be seen from the distance plots that PNS in both the *C*-PNS and *P*-PNS orientations can form inclusion complexes well with all five different CDs. The two important factors, *(i)* the substitutions on 2- and 6-positions of βCD and *(ii)* the mode of PNS binding, are likely to be involved in the mobility and preferential displacement of PNS inside the hydrophobic cavity of CDs. Where the same substitutions on both 2- and 6-positions of βCD (i.e., βCD, 2,6-DMβCD, and 2,6-DHPβCD), the *C*-PNS stably positioned nearby the secondary rim (~3 Å), while *P*-PNS preferred a deeper location and showed a higher movement along the simulation due to a reduced fitting of its benzene ring within the cavity. As 2-hydroxypropyl substitutions on the 2- or 6-position of βCD (2-HPβCD or 6-HPβCD), the hydrophilic functional groups significantly induced PNS displacement to be relatively nearer to the substituted rim. In 2-HPβCD, the PNS molecule initially moved up over 4 Å and then moved down to be steadily located at ~3Å until the end of simulations. Although the large fluctuation of both the *C*-PNS and *P*-PNS binding modes were observed in 6-HPβCD, a more than 50% occupation of PNS was found at the position below the center of gravity of 6-HPβCD.

3.1.1.4 Water accessibility to PNS in complex with CDs

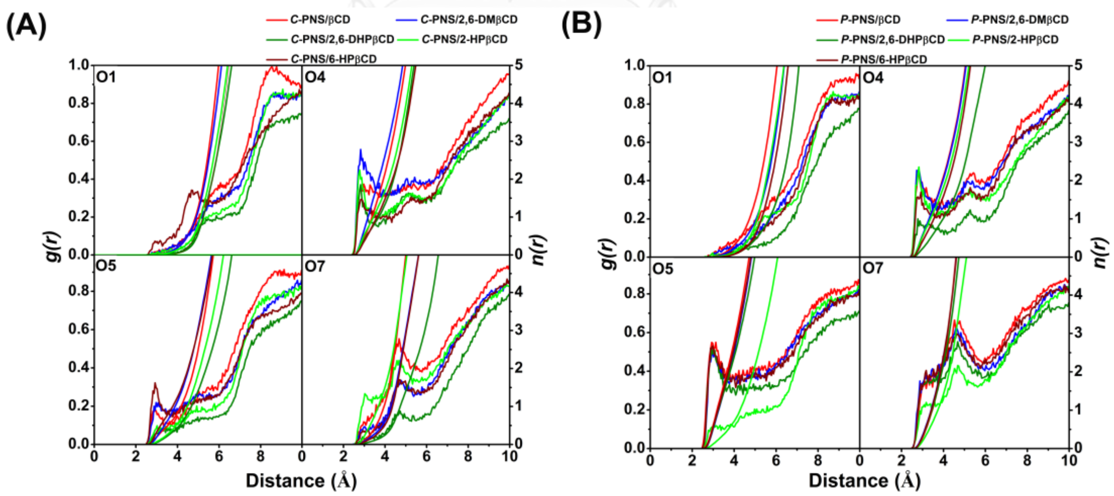

Fig. 6 The radial distribution function (RDF) of water molecules around the PNS oxygen atoms (as defined in Fig. 1) for (A) *C*-PNS/CDs and (B) *P*-PNS/CDs inclusion complexes.

The radial distribution functions (RDFs) were used to ascertain the water distribution around the four oxygen sites on the chromone ring of the PNS molecule (O1, O4, O5 and O7) (Fig. 1) in complex with the different CDs. The RDFs of these PNS oxygen atoms together with the integration number, *n(r)*, for the different *C*-PNS/CD and *P*-PNS/CD inclusion complexes are plotted in Fig. 6. The *n(r)* value at the first determined minima was used to estimate the water accessibility towards the focused oxygen, and the results are summarized in Table 1. Amongst the four sites, no peak was detected within the 3 Å sphere of the O1 site in all systems (except for only a rather small peak found in C-PNS/6-HPβCD). These data suggested that water hardly solvates these oxygen atoms of the chromone ring reflecting that it mostly stayed inside the center of the hydrophobic cavity of the respective CDs. An unpronounced peak was observed at around 2.7-4.0 Å for the O7 methoxy oxygen atom indicating a weak solvation or an O7-water interaction. In contrast, the two other sites exhibited the first intense peak at ~3 Å, corresponding to possible hydration, while the first minima accounted for a number of water molecules maintained on the first hydration shell. Since the first minima never reached a *g(r)* value of zero, water exchange between the first and secondary hydration shells was feasible. In *C*-PNS/CDs inclusion complexes, the O4 oxygen was more accessible to water than the O5 and O7 ones, in agreement with the *C*-PNS displacement nearby the secondary rim where O5 and O7 atoms of the chromone ring were located a little bit deeper in the cavity than O4. Interestingly, lower water accessibility was seen in the *C*-PNS/2,6-DHPβCD complex due to 2-hydroxypropyl substitutions on both CD rims. For the *P*-PNS binding mode, the chromone ring of *P*-PNS stayed close to the wider rim and so a ~two-fold higher water accessibility was observed (Table 1). Since both

C-PNS and *P*-PNS/CDs complexes with the different βCD could be formed (evidently from the distance plot) with an almost equal binding strength (discussed later in Fig. 7), the total number of accessible water molecules could be considered for both complexes. Considering the average total number of water molecules solvating the PNS bound to each respective CD, it appears that 2,6-DMβCD introduced one more solvated water, but ~1-2 less water molecules approached PNS when complexed with 2,6-DHPβCD and 2-HPβCD compared to when complxed with βCD.

Table 1 Integral number, *n(r)*, up to the first minimum (derived from Fig. 5) for the PNS oxygen atoms in the different PNS/CDs complexes

	βCD		**2,6-DMβCD**		**2,6-DHPβCD**		**2-HPβCD**		**6-HPβCD**	
	***C*-PNS**	***P*-PNS**	***C*-PNS**	***P*-PNS**	***C*-PNS**	***P*-PNS**	***C*-PNS**	***P*-PNS**	***C*-PNS**	***P*-PNS**
O1	-	-	-	-	-	-	-	-	-	-
O4	1.5	2.3	3.5	1.4	0.9	1.0	1.4	1.3	0.9	1.5
O5	0.5	2.5	0.8	2.0	-	2.5	-	0.5	0.9	2.7
O7	-	1.3	0.3	2.5	-	1.7	0.8	1.1	0.1	1.7
Total	2.0	6.1	4.6	5.9	0.9	5.2	2.2	2.9	1.9	5.9
Average	4.0		5.2		3.0		2.5		3.9	

3.1.1.5 Binding free energy of inclusion complex

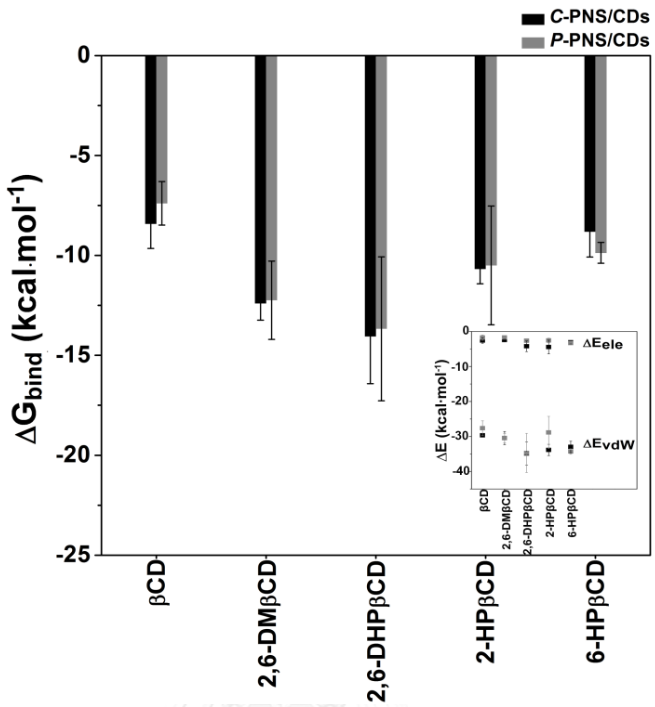

Fig. 7 MM/GBSA binding free energy (ΔG_{bind}) in kcal/mol of the different *C*-PNS/βCD (black) and *P*-PNS/βCD (grey) complexes, where the interaction energy components, ΔE_{ele} and ΔE_{vdW}, are given in the inset

To estimate the binding free energy or the absolute free energy of molecules in aqueous solution (ΔG_{bind}) for all PNS/βCDs inclusion complexes, the MM-GBSA approach [69] was performed on the 30 MD snapshots extracted from the last 40 ns. It has to be noticed that four sets of 100, 30, 20 and 10 snapshots were investigated and the 30 snapshots yielded the relative magnitude of mean and standard deviation values of the 100 snapshots. Based on MM-GBSA calculations, ΔG_{bind} is the summation of the electrostatic (ΔE_{ele}) and van der Waals (ΔE_{vdW}) interaction energies in gas phase, GBSA solvation free energy [70], and entropy contribution using normal mode analysis [71]. The ΔG_{bind}, E_{ele} and E_{vdW} values of *C*-PNS and *P*-PNS in complex with the different βCDs are presented and compared in Fig. 7. Although the structural and dynamic behaviors, as well as water accessibility, of the two modes of PNS binding in the cavity were somewhat distinguishable, the difference in their binding free energies was less than 2 kcal/mol. Importantly, the averaged ΔG_{bind} values (kcal/mol) suggested that the modification of βCD by both methyl and 2-hydroxylpropyl groups could enhance the stability of inclusion complex in order of 2,6-DHPβCD (-13.86) >2,6-DMβCD (-12.32) >2-HPβCD (-10.59) >6-HPβCD (-9.34) >βCD (-7.90). As expected for the complex formation of phenolic compounds dipping into the hydrophobic inner surface, vdW interaction plays an important role in the complexation process, and they appear to be much stronger than the electrostatic interaction. It turned out to be approximately 6-fold in the case of PNS/CDs complexes.

3.1.2 Steered Molecular dynamics (SMD) simulation

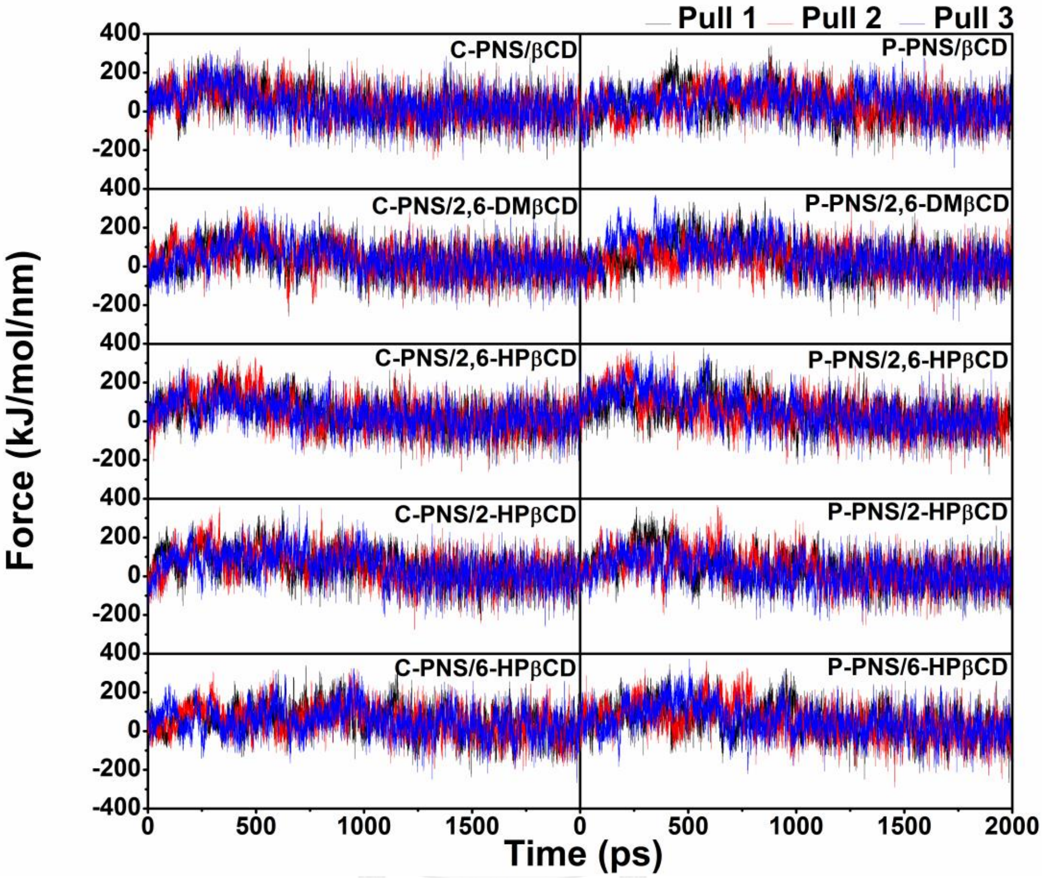

Fig. 8 Force for pulling ligand passed through the wider rim of each βCD inclusion complexes along simulation time

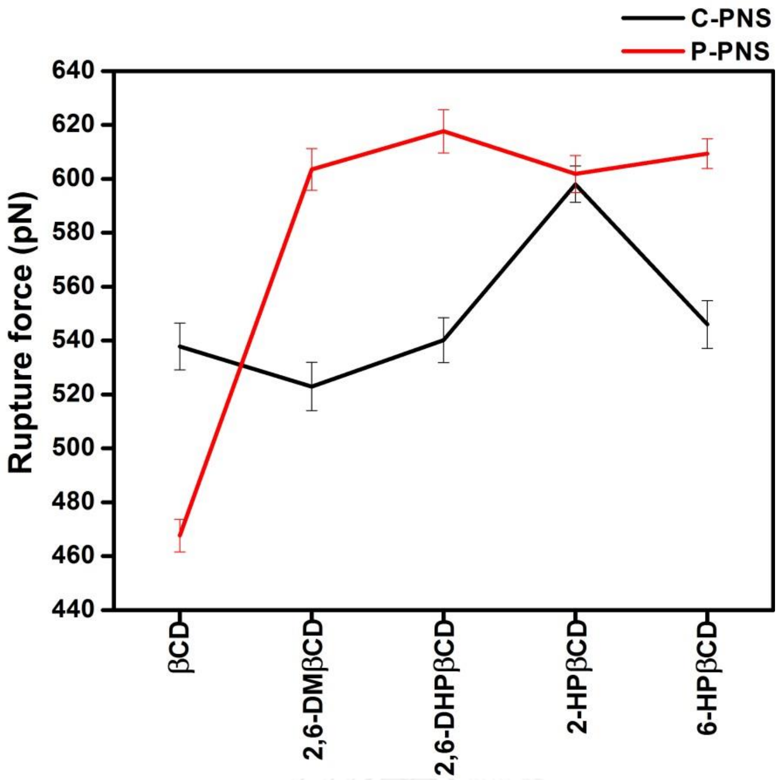

Fig. 9 Rupture force (F_{max}, pN) derived from the force-time profile of pulling the two oriented ligands, *C*-PNS and *P*-PNS, out from the wider rim along the host cavity axis (z-direction) for each inclusion complex

Nowadays, Steered Molecular Dynamics (SMD) simulations was a flexible and powerful tool that was plentifully used in the scientific research in order to understand the ligand-protein recognition, investigate the dynamic behavior of biological system and also obtained to primarily design the new structure-based drug [72-74]. In this work, SMD was obtained to understand the molecular interaction by monitoring the rupture force the derived from the profile of pulling the guest molecule (PNS) out of βCDs cavity. As initial, PNS was located in hydrophobic cavity of βCD and its derivatives. PNS was then pulled out of the cavity by outer force along Z-axis. The pulling simulations were performed at the same spring constant. Along the simulations for all complexes (Fig. 8), the pulling force reached the maximum value approximately at 500 ps, when PNS molecule escaped from the nanocavity and the intermolecular interaction between PNS and βCDs which was the Vdw interaction was broken. The results were in somewhat correspondence with the SMD study on progesterone/βCD complex [75]. Based on the hypothesis of a higher pulling force applied for a more favorable binding mode of guest molecule in complex with individual CD, *P*-PNS preferably interacted with 2,6-DMβCD, 2,6-DHPβCD, 6-HPβCD and in *vice versa* for parental βCD, whilst both orientations of *P*-PNS and *C*-PNS were almost equally favorable to bind with 2-HPβCD. The F_{max} values in order of 2,6-DHPβCD (618 pN) > 6-HPβCD (609 pN) > 2,6-DMβCD (603 pN) ~ 2-HPβCD (601 pN) > βCD (468 pN) also pointed out the improved stability of PNS by forming an inclusion complex with the modified βCDs better than βCD one discussed later in the phase solubility study. The obtained results described that the difference in pulling force and binding strength can be due to guest orientation occupied inside the host cavity [50].

3.2 Experiments

3.2.1 The maximum absorption of Pinostrobin by spectrophotometry

The solution of free compound of PNS, three β-cyclodextrins (βCD, 2,6-DMβCD and HPβCD) and the three inclusion complexes (PNS/βCD, PNS/2,6-DMβCD and PNS/HPβCD), which were prepared by freeze dried, were dissolved in deionized water. After that, the absorption in the range of 200-400 nm was monitored by spectrophotometry. The spectrophotometry was performed for basic analysis of PNS because this method is rather convenient, quick and cheap. Absorption maximum wavelength of free compound of PNS was observed at 290 nm (Fig. 10). Also, the inclusion complexes of PNS had the same absorption maximum wavelength at 290 nm and the maximum wavelength peak was not shifted after complex formation. In case of βCD and its derivatives, they had no UV absorption because they were not comprised of the functional group that can be absorbed in the UV range [76]. Consequently, PNS concentration was then measured at 290 nm in this study.

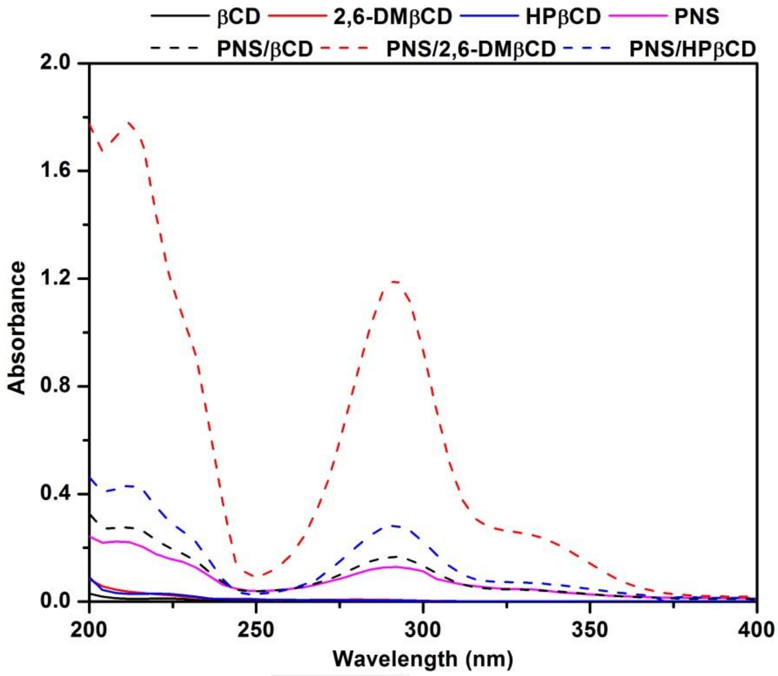

Fig. 10 The UV spectrum of free compound of PNS, β-cyclodextrins (βCD, 2,6-DMβCD, HPβCD) and its inclusion complexes (PNS/βCD, PNS/2,6-DMβCD and PNS/HPβCD)

3.2.2 Standard curve of Pinostrobin by spectrophotometry

The standard curve of PNS was plotted between absorbance at 290 nm that was the maximum wavelength of PNS and the various concentrations of PNS in the range of 0 to 0.1 mM. According to Fig. 11, the regression coefficient of linear relationship was highly correlated (R^2= 0.997).

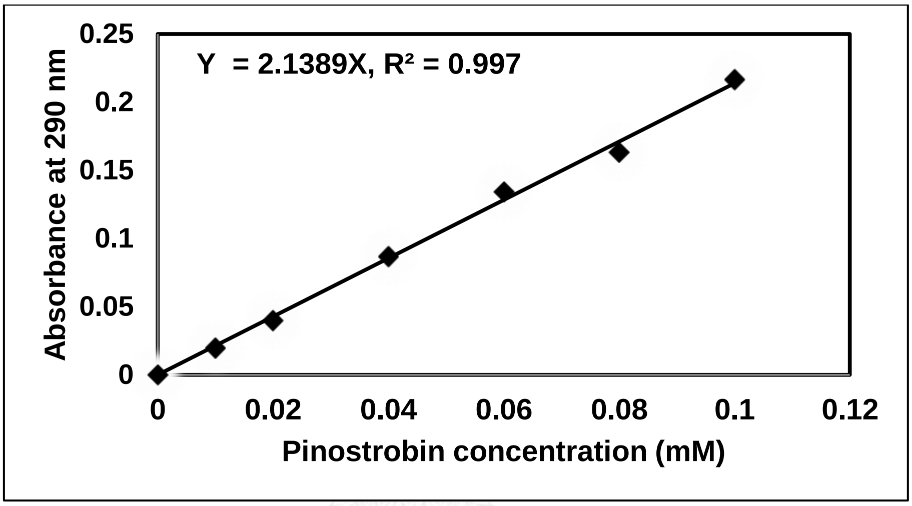

Fig. 11 Standard curve of PNS by spectrophotometry

3.2.3 Standard curve of Pinostrobin by High Performance liquid chromatography

Before creating the standard curve of PNS by HPLC, the retention time (R_t) of PNS was detected by dissolved free compound of PNS and its freeze-dried inclusion complexes in milli Q water and following the method described in 2.5.5. Then the sample solutions at the time of 240 minutes were chosen to determine their retention time by reverse phase C 18 HPLC with UV detector at 290 nm. In addition, Wu and co-worker also determined PNS concentration by High Performance Liquid Chromatography (HPLC) at the wavelength of 290 nm [15]. According to Fig. 12, the retention time of PNS with- and without βCDs complexation was at ~28 minutes. Thus, the peak area at R_t equal to 28 min was plotted against the final concentration from 0 to 0.15 mM of free compound of PNS which were dissolved and serial diluted in milli Q water. From the standard curve of PNS detected by HPLC (Fig. 13), the regression coefficient of the linear relationship was highly significant (R^2 = 0.9864) and the linear equation could be used for calculating the concentration of PNS in further analysis.

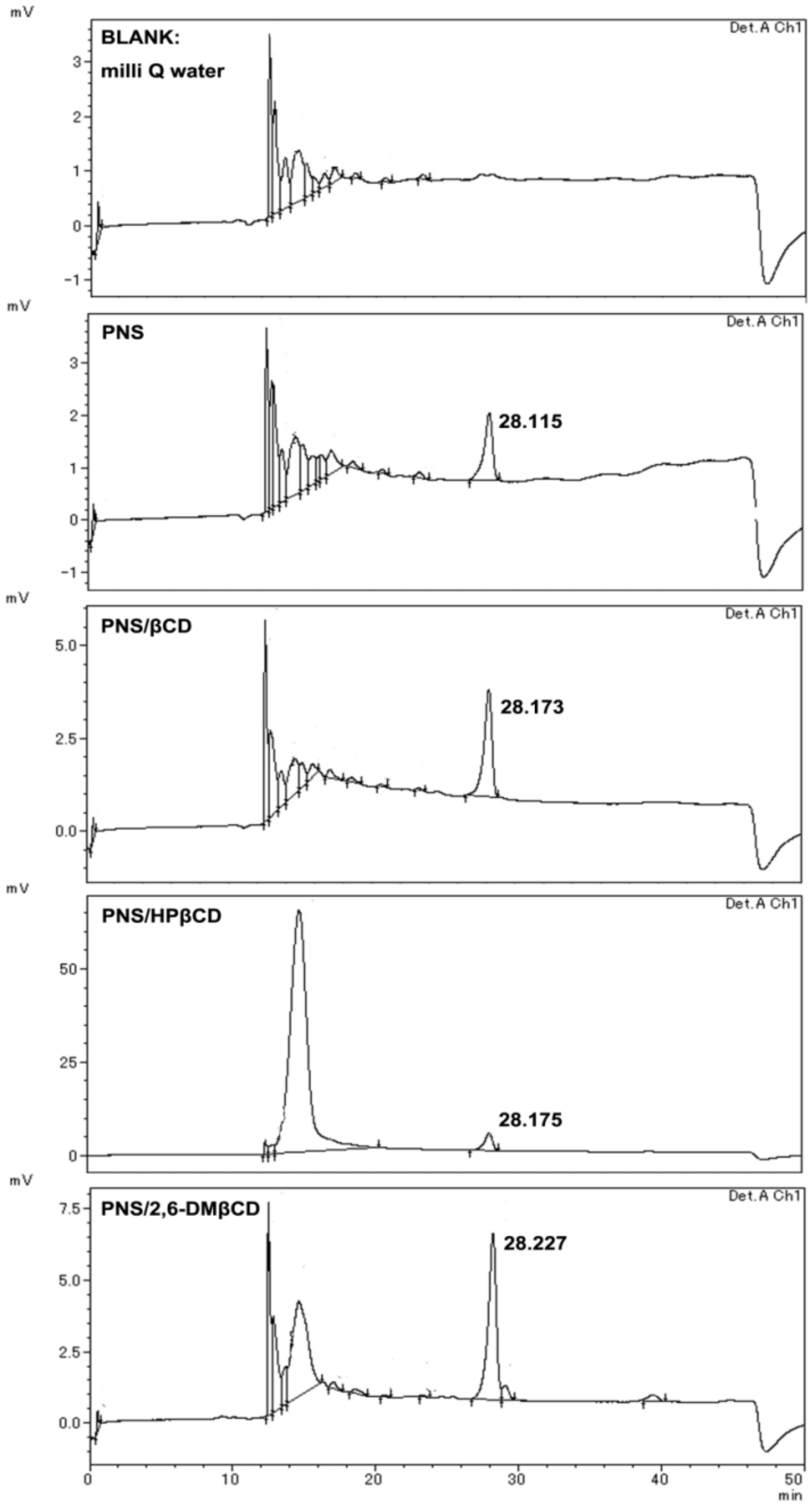

Fig. 12 HPLC profile on a reverse phase C_{18} column of free compound of PNS and its inclusion complexes that were dissolved in milli Q water (Blank was milli Q water). Elution was by 70:30 MeOH:Milli Q water

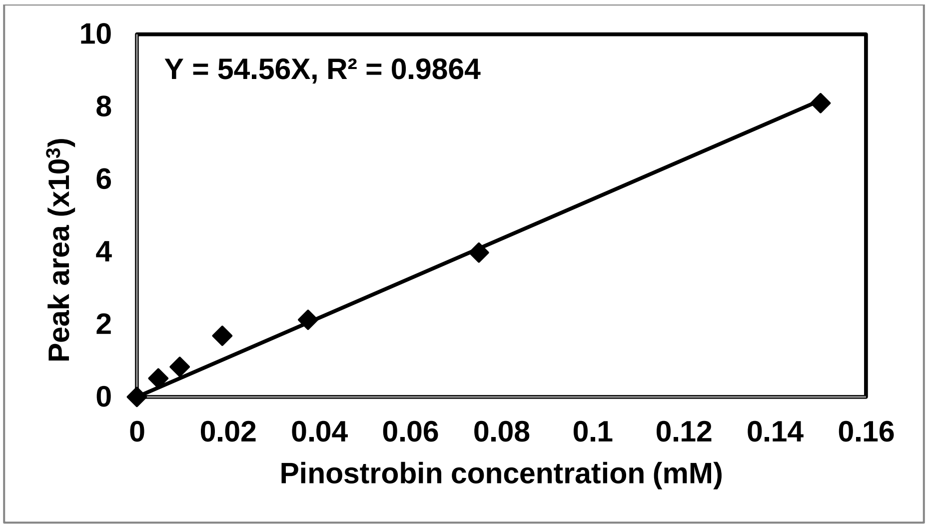

Fig. 13 Standard curve of PNS by HPLC

3.2.4 Phase-solubility diagram

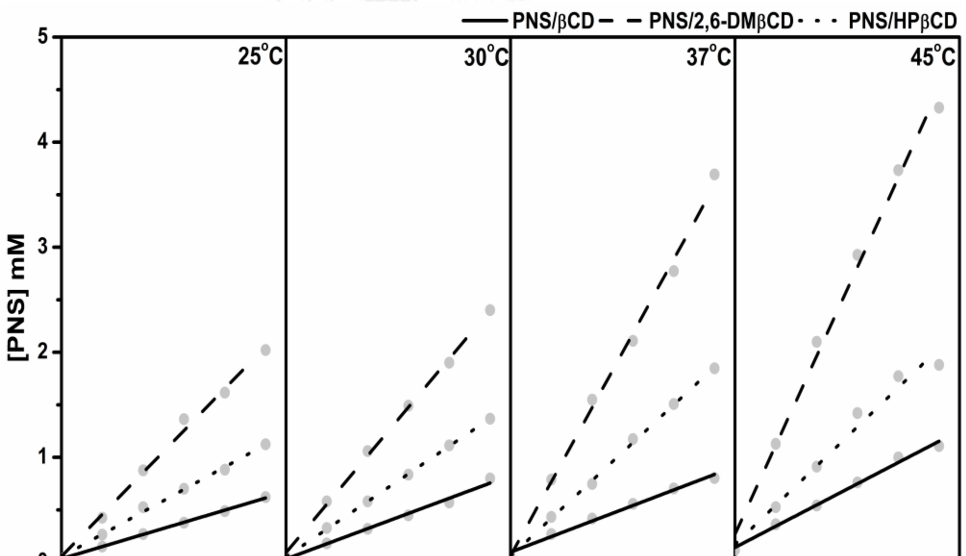

Fig. 14 Phase solubility diagram for PNS in various concentrations of (—) βCD, (−−−) 2,6-DMβCD and (⋯⋯) HPβCD at different temperatures

Table 2 Slope, correlation coefficient (r^2) and stability constant (K_C) of PNS/βCDs complexes (derived from Fig. 14)

Temperature (°C)	βCD	S_0 (mM)	*slope*	r^2	K_C (M^{-1})
25	βCD	0.034	0.058	0.999	1799
	2,6-DMβCD		0.200	0.994	7322
	HPβCD		0.107	0.996	3503
30	βCD	0.049	0.072	0.989	1575
	2,6-DMβCD		0.231	0.998	6074
	HPβCD		0.132	0.999	3070
37	βCD	0.071	0.084	0.999	1301
	2,6-DMβCD		0.348	0.999	7562
	HPβCD		0.167	0.997	2843
45	βCD	0.096	0.103	0.996	1191
	2,6-DMβCD		0.400	0.995	6934
	HPβCD		0.186	0.996	2373

S_0 was the concentration of PNS in deionized water that was measured without any βCDs.

The selected properties of inclusion complexes between βCDs and guest molecule can be determined by determining the effect of βCDs concentration on the guest molecule solubility. The slopes that were derived from phase solubility diagram and the intrinsic solubility of guest molecule can provide information about the type of complex formation (stoichiometry) and its stability constant.

The phase solubility studies were performed according to the method of Higuchi and Connors to evaluate the effect of βCDs on the solubility of guest molecule (PNS). In this experiment, excess amount of PNS were added to the various concentration solutions of βCDs which were incubated at different temperature to determine the solubility type and molar ratio of the inclusion complex. As the result, the phase solubility diagrams in Fig. 14 showed a linear relationship which could be classified as A_L-type. It was clearly observed that solubility of PNS increased with increasing concentration of βCDs, the stoichiometric molar ratio of PNS/βCDs inclusion complex should be 1:1. The system of PNS/2,6-DMβCD showed higher solubility than PNS/HPβCD and PNS/βCD, respectively. It indicated that 2,6-DMβCD and HPβCD can enhanced the solubility of PNS better than the parental βCD suggesting the effect of methyl- and hydroxyl- groups. In addition, the higher solubility could be due to the substituent group of βCD derivatives that can increase the possibility of guest molecule to interact with water molecule [30]. The phase solubility of various guest molecules with βCD and its derivatives has been reported in several studies [30, 77]. For example, the phase solubility of artesunate was the A_L type diagram which illustrated the soluble 1:1 complexes. The work also suggested that the solubility of the guest molecule was raised by the ability of each cyclodextrin in the order of methyl-βCD > HPβCD > βCD [77].

Furthermore, the stability constant (K_C) of each inclusion complex was calculated from Eq. 9, the slope value was determined from the diagram while the intrinsic solubility of PNS (S_0) which were the concentration of PNS in deionized water without any βCD at each temperature was obtained by independent measurement. The calculated stability constants were quite sensitive to the PNS intrinsic solubility (S_0) because the intercept of the diagrams could not be certainly measured due to low solubility of the free guest. In addition, the stability constant reflects binding behaviors between guest and host molecule. The strong binding had higher K_C value than the weak binding. According to Table 2, the K_C of PNS in 2,6-DMβCD was higher than those in HPβCD and βCD at all temperatures measured. Thereby, it can be assumed that PNS was strongly bound to the 2,6-DMβCD when compared to HPβCD and βCD, respectively. The binding behaviors still showed the same trend at the temperatures from 25 to 45 °C. The results implied that the 2,6-DMβCD complex was more stable than the other two complexes.

3.2.5 The Van't Hoff Plot

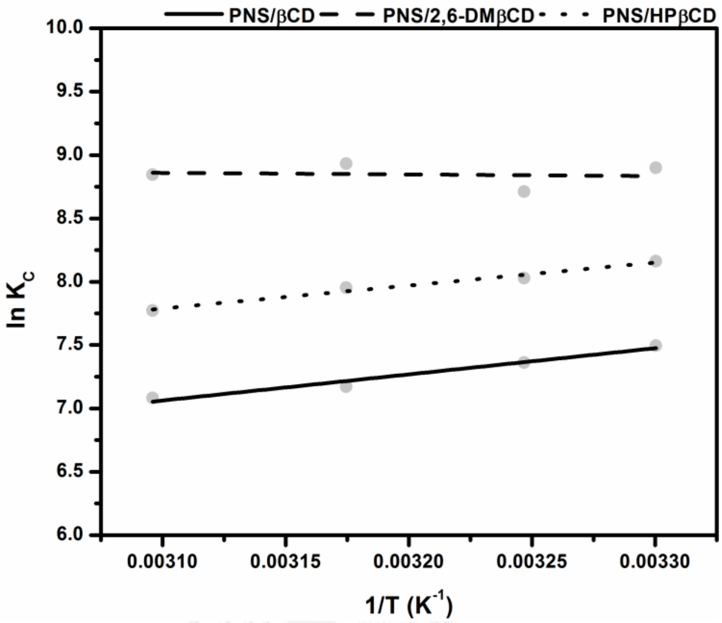

Fig. 15 The Van't Hoff plot of the (—) PNS/βCD, (–––) PNS/2,6-DMβCD and (······) PNS/HPβCD inclusion complex

Table 3 Thermodynamic values of the three inclusion complexes (derived from Fig. 15)

Inclusion complex	$\Delta H^{\mp}$ (kJ mol^{-1})	$T\Delta S^{\mp}$ (kJ mol^{-1})	$\Delta G_{25}^{\mp}$ (kJ mol^{-1})
PNS/βCD	-17.15	1.66	-18.81
PNS/2,6-DMβCD	1.04	22.91	-21.87
PNS/HPβCD	-15.08	5.37	-20.45

The Van't Hoff (Fig. 15) was plotted in order to observe an influence of temperature on the stability of the complexes and examine the thermodynamic properties of the inclusion process.

According to Tommasini et al [37], the integrated form of Van't Hoff as Eq. (12) was suggested to calculate the thermodynamic parameters. The enthalpy ($\Delta H^{\mp}$) and entropy ($\Delta S^{\mp}$) of the inclusion process were obtained by plotting the stability constant (K_C) in Table 2 against the reciprocal temperature using Eq. (12), while the Gibbs free energy at 25 **°C** ($\Delta G_{25}{}^{\mp}$) was evaluated by Eq. (13). The thermodynamic parameters for all three PNS/βCDs were summarized in Table 3.

$$\ln K_C = -\frac{\Delta H^{\mp}}{RT} + \frac{\Delta S^{\mp}}{R} \tag{12}$$

$$\Delta G_{25}{}^{\mp} = \Delta H - T\Delta S \tag{13}$$

The thermodynamic parameters can be calculated from the linear profiles of the Van't Hoff plot. The values of thermodynamic parameters were shown in Table 3. The large negative enthalpy energies of -17.15 and -15.08 kJ/mol for PNS/βCD and PNS/HPβCD suggested that the complex formation was likely associated with an enthalpy driven through exothermic process. This is in contrast for PNS/2,6-DMβCD complexation formed via small endothermic process controlled by entropy driven (a slightly positive enthalpy of 1.04 kJ/mol and a large positive entropy term of 22.91 kJ/mol) [19]. This principally positive entropy value suggests the loose fit of PNS inside 2,6-DMβCD cavity, causes a higher translational and rotational degrees of freedom of the 2,6-DMβCD which can cause lead to the inward movement of water moiety surrounding the PNS molecule [78]. From the Gibbs free binding energy of host and guest molecules estimated by a summation of enthalpy and entropy terms, all spontaneously formed inclusion complexes were described by the negative value of $\Delta G_{25}^{\mp}$ with the following order of complex stability or binding strength: PNS/2,6-DMβCD (-21.87 kJ/mol) > PNS/HPβCD (-20.45 kJ/mol) > PNS/βCD (-18.81 kJ/mol).

3.2.6 Characterization of solid inclusion complexes

3.2.6.1 Differential Scanning Calorimetric analysis (DSC)

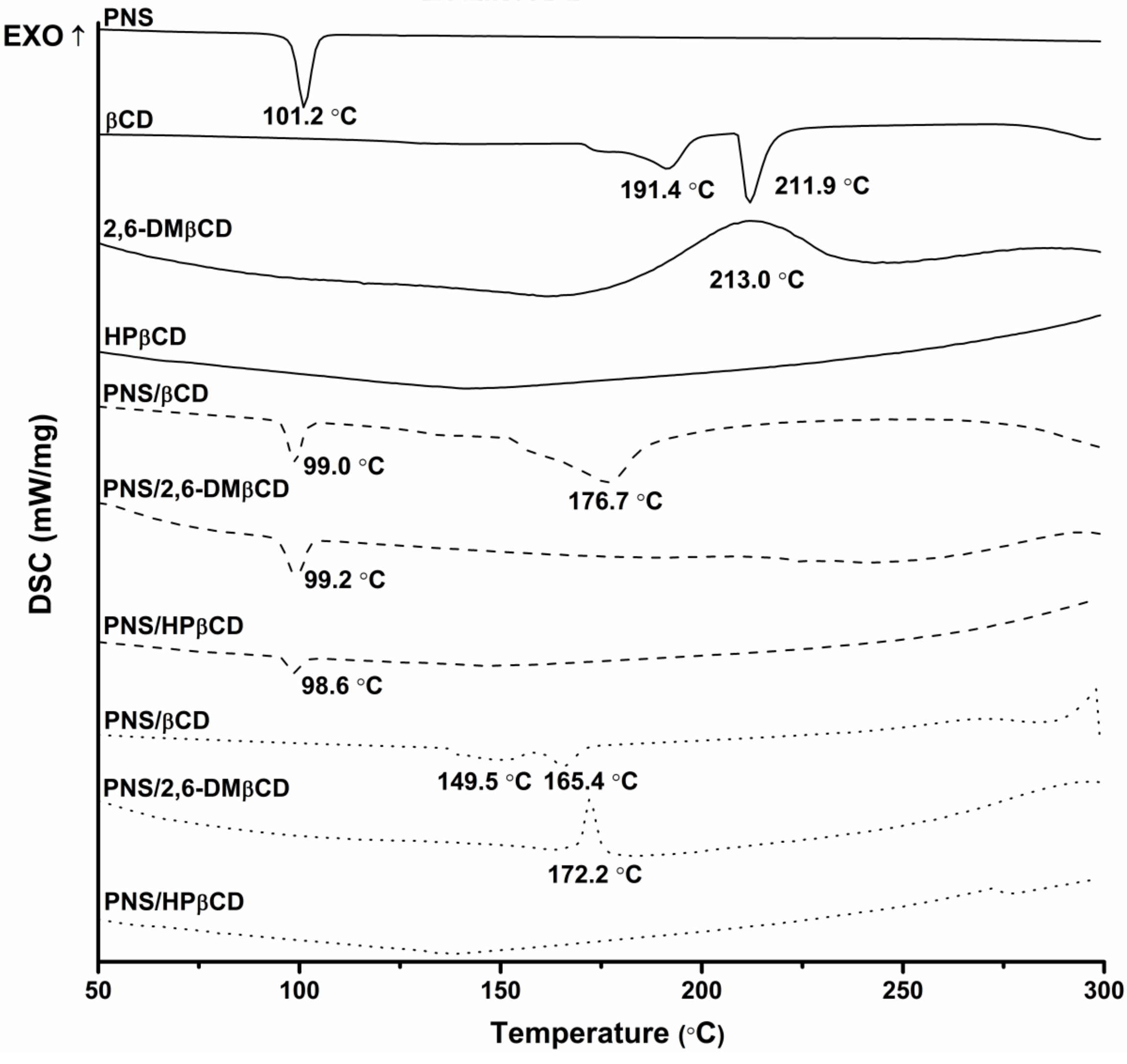

Fig. 16 DSC thermogram of free PNS and the inclusion complexes

In this study, the Differential Scanning Calorimetry or DSC was applied in order to preliminary investigate the thermal behavior of free guest compound and the inclusion complexes. DSC was widely used for physicochemical characterization of inclusion complex formation in the solid state. From the DSC thermograms (Fig. 16), there are the thermograms of free PNS, βCD, 2,6-DMβCD and HPβCD (solid line), and of the products that were prepared by physical mixture (dash line) and freeze-drying methods (dot line), respectively. The sharp endothermic peak of free PNS was observed at 101.2 °C which could be referred to its melting point. The thermograms of free βCD showed the prominent endothermic peak at 211.9 °C while 2,6-DMβCD and HPβCD displayed the broad peak at 213 °C and approximately at 134 °C, respectively. The distinct melting endotherm peak of free PNS was expressed at approximately 99 °C in physical mixture products. This suggested that the physical mixture was not a true inclusion complex since there seem to be a superimposition between free compound of PNS and βCDs. Liu and co-worker suggested that the physical mixture was simply a mixing of the two compounds and it was not a genuine complex, thus the luteolin endothermal peaks were found in their study [79]. On the other hand, the sharp endothermic peak of free PNS was completely disappeared in the freeze-dried products. Also, the thermal peaks of βCD and its derivatives were shifted and decreased in intensity. The true inclusion complex formation could be demonstrated by freeze-dried products due to the replacement of water by PNS and the reduction of the maximum dehydration peak [80]. Our result agrees well with Wang's work [81] in which a true complex was observed from the freeze-dried product between quinestrol and 2,6-DMβCD.

3.2.6.2 Two-dimensional Nuclear Magnetic Resonance (ROESY-NMR)

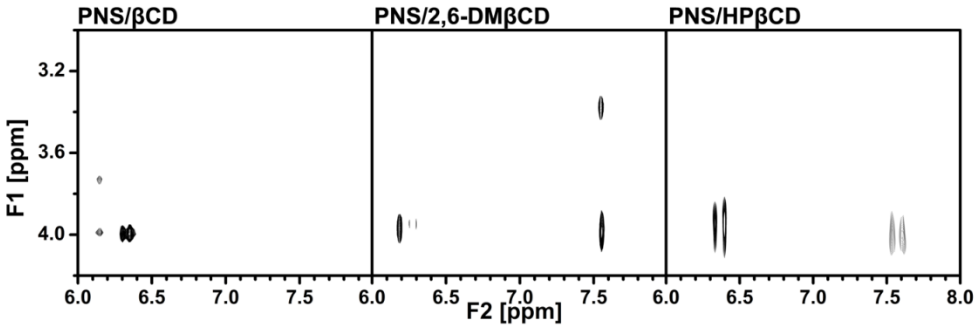

Fig. 17 2D ROESY NMR spectra of the freeze-dried inclusion complexes between PNS and βCDs (F1= ^{1}H NMR of βCDs and F2=^{1}H NMR of PNS)

Further information on the geometry of the guest molecule inside βCDs cavity was investigated by two dimensional NMR (2D-ROESY). 2D-ROESY NMR is a powerful tool that was examined to clarify the configuration of PNS in the βCD and its derivatives cavity. A partial contour plot of proximities between protons of PNS and βCDs were shown in Fig. 17. From the PNS/βCD inclusion complex, the intermolecular cross-peak between H-3 of βCD (~4 ppm) and H-6 or H-8 of PNS (6.2-6.4 ppm) which is a part of chromone ring was shown. Whilst the βCD derivative inclusion complexes had an additional correlation peak that was the cross-peak between H-3 of βCD derivatives (~4 ppm) and H-2', H-3' and H-4' of PNS (7.5-7.7 ppm) which is a part of phenyl ring. Especially, in case of 2,6-DMβCD inclusion complex, the intermolecular cross-peak between 2-OCH_3 of 2,6-DMβCD (~3.4 ppm) and phenyl ring (7.5-7.7 ppm) was also found. These results indicated that the parental βCD inclusion complex had one orientation that was a chromone ring inside the cavity. However, the βCD derivatives inclusion complexes had two orientations of PNS inside the cavity, either the chromone- or phenyl- part. In addition, the phenyl ring of PNS might strongly interact with the 2,6-DMβCD since both 2-OCH_3 and H-3 of 2,6-DMβCD could be interacted. In the previous work, the two different types of the inclusion complex between HPβCD and epigallocathechingallate were formed [82].

3.2.7 Analysis of dissolution diagram of the inclusion complexes

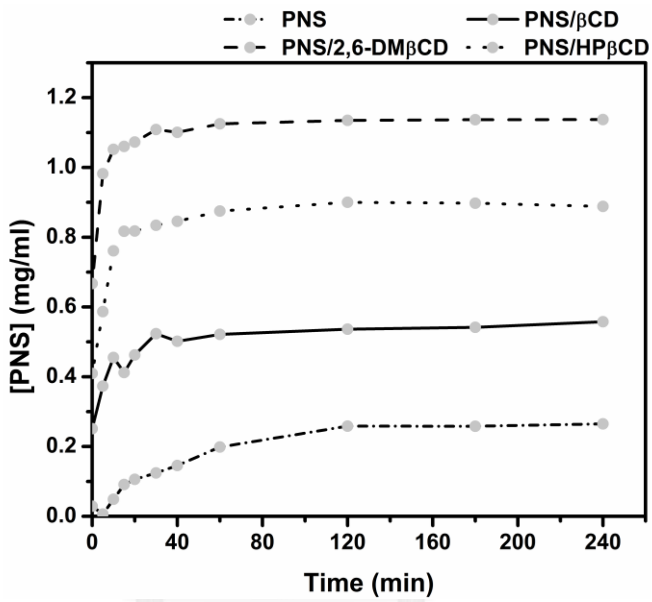

Fig. 18 Dissolution diagram of free PNS and its inclusion complexes in water at 37 °C

In vitro dissolution study is necessary for elucidation of the dissolution behaviors of new developed medicines. It is the widely accepted method that is usually performed in the pharmaceutical field [44, 83, 84]. In this research, the dissolution profile of free PNS and its freeze-dried complexes with βCDs were carried out in water at 37 °C for 240 minutes and the concentration of PNS was detected by HPLC. The dissolution of free PNS was compared with the three inclusion complexes (PNS/βCD, PNS/2,6-DMβCD, PNS/HPβCD) by plotted the concentration of PNS in the interval times. From the diagram in Fig. 18, the free PNS was poor when compared with the inclusion complexes. The inclusion complexes exhibited a faster dissolution rate than free PNS in the initial phase. After 15 minutes, the amount of free PNS was dissolved 0.09 mg/ml and the PNS in the inclusion complexes with βCD, 2,6-DMβCD and HPβCD were 0.41, 1.06 and 0.82 mg/ml, respectively. The result exhibited that the modified βCD inclusion complexes had a higher dissolution rate than parental βCD. The reason for this could be the $-OCH_3$ group of 2,6-DMβCD had higher ability to interact to water molecule, and hydroxypropyl modified βCD in HPβCD can form more H-bond and might reduce the aggregation behavior in water [85]. In spite of that, among the βCDs, 2,6-DMβCD seems to be the best carrier host as described in previous works [86, 87]. From the recent work, the effect of cyclodextrins on aqueous solubility of a flavonoid apigenin was evaluated. They suggested that random methyl-βCD can enhance the solubility of apigenin better than the HPβCD and parental βCD. Furthermore, their results confirmed that the derivatives of βCDs would be essentially useful in further drug delivery systems containing flavonoids [83].

3.2.8 Determination of biological activity of inclusion complexes

3.2.8.1 Anti-inflammatory assay

Table 4 Anti-inflammatory effect of PNS and its βCDs complexes as well as cytotoxic effect towards HeLa and MCF-7 cells as indicated by the IC_{50} value

	IC_{50} [µM]		
	IL-6 secretion	Cytotoxicity Hela	Cytotoxicity MCF-7
PNS	30	79	22
PNS/βCD	61	72	28
PNS/2,6-DMβCD	49	95	18
PNS/HPβCD	27	65	29

According to the previous work on the effect of the free PNS on nitric oxide, cyclooxygenase-1 and 2 induced by LPS/IFN-γ in RAW 264.7 cells is not significant [88]. In our work, the murine macrophage cell line (RAW 264.7) was stimulated by LPS and co-treated with free PNS and the three inclusion complexes (PNS/βCD, PNS/2,6-DMβCD and PNS/HPβCD). PNS and its complexes significantly exerted a lowering effect on the IL-6 secretion in LPS-stimulated macrophages. In fact, the IC_{50} values were comparable for PNS (30 µM) and PNS/HPβCD (27µM) (Table 4). For PNS/2,6-DMβCD and PNS/βCD the IC_{50} was slightly higher with 49 µM and 61 µM, respectively.

3.2.8.2 Cytotoxicity assay

The effect of PNS on many cancer cell lines has previously been reported [89, 90]. Especially, leukaemia cell line, neoplastic disease of bone marrow or also known as white blood cell cancer was potentially inhibited by PNS [91, 92]. However, the influence of PNS and its inclusion complexes on the cancer cell lines HeLa (cervical cancer cell line and MCF-7 (breast cancer cell line) has not been widely reported yet. Therefore, in the study the cytotoxicity effect of PNS and its inclusion complexes (PNS/βCD, PNS/2,6-DMβCD and PNS/HPβCD) on this cancer cell lines was investigated. According to Table 4, the free compound and its complexes had a significant effect on the HeLa with an IC_{50} value of 79 µM for the free PNS and IC_{50} values ranging between 65 and 95 µM for the complexes. Thus the cytotoxic effect of the complexes is slightly, but not significantly different compared to the complexes. Regarding the MCF-7 cell line, PNS is more cytotoxic in relative to the HeLa cell lines with an IC_{50} value of 22 µM. Again, the effect of the complexes is not significantly different with the values between 18 and 29 µM.

CHAPTER IV

CONCLUSIONS

In the MD simulations the stability of simulated systems of each PNS/βCD inclusion complex reached equilibrium by 40 ns and was then used to investigate the conformations of βCD and its derivatives, the mobility of the host PNS molecule in the different PNS/βCD complexes, the water accessibility around PNS and the binding free energies of each inclusion complex. The results revealed that the conformation of βCD and its derivatives complexed with PNS is mostly found in M1 structure of the PES. By means of the PNS mobility, the chromone ring of the PNS molecule preferably stays nearby the secondary rim of βCD and its derivatives, while another orientation of the PNS molecule the phenyl ring shows a higher movement inside the hydrophobic cavity. In addition, the RDF plots show that PNS in the different *P*-PNS/βCD inclusion complexes interacts with ~two-fold more solvating water molecules than in the different *C*-PNS/βCD inclusion complexes. It could then be assumed that the *P*-PNS/βCD inclusion complexes have a better water solubility than the corresponding *C*-PNS/βCD ones. According to the binding free energy, van der Waals interaction is the most important interaction between the PNS and the βCD or its derivatives. The PNS complex with 2,6-DHPβCD had the highest stability, followed by the inclusion complexes with 2,6-DMβCD, 2-HPβCD, 6-HPβCD and βCD, respectively. Moreover, experimental phase solubility studies supported the computational approach since complexes of PNS/2,6-DMβCD and PNS/HPβCD showed a significant higher stability than those with βCD at all examined temperatures. The solubility of host-guest inclusion complex of PNS with βCD and its derivatives was A_L type. It could be described that PNS solubility increased when increasing the concentration of βCDs. The DSC thermograms of freeze-dried inclusion complexes showed completely disappeared endothermic peak of PNS that could indicate that freeze drying method can be used to prepare the true inclusion complex. Moreover, two-dimensional NMR (2D-ROESY NMR) was employed to clarify the binding mode of PNS in cavity of βCD and its derivatives. The NMR spectrum revealed that *P*-PNS and *C*-PNS were located inside βCD derivatives whereas *C*-PNS was only found to interact with parental βCD. The results of SMD were in good agreement with MDs and also phase solubility. According to the dissolution profile, the amount of PNS dissolved was in the order of PNS/2,6-DMβCD > PNS/HPβCD > PNS/βCD > PNS. The IC_{50} exhibited that PNS and its complexes had a lowering effect on the IL-6 secretion in LPS-stimulated macrophages. *In vitro*, PNS in complex with and without βCDs showed a moderate cytotoxic effect against HeLa and MCF-7 cancer cell lines.

REFERENCES

1. Sher, A., ***Antimicrobial activity of natural products from medical plants*** Gomal J Med Sci., 2009. **7**: p. 72-78.

2. Beecher, G.R., ***Overview of dietary flavonoids: nomenclature, occurrence and intake*** J. Nutr., 2003. **10**: p. 3248S-3254S

3. J.V. Formica, W.R., ***Review of the biology of quercetin and related bioflavonoids*** Food Chem Toxicol., 1995. **33**: p. 1061-1080.

4. P.C.H. Hollman, M.B.K., ***Absorption, metabolism, and health effects of dietary flavonoids in man*** Biomed Pharmacother., 1997. **51**: p. 305-310.

5. C.A. Rice-Evans, N.J.M., G. Paganga ***Structure antioxidant activity relationships of flavonoids and phenolic acids*** Free Radic., 1996. **20**: p. 933-956.

6. K.A. O'Leary, S.P.-T., P.W. Needs, Y.P. Bao, N.M. O'Brien, G. Williamson ***Effect of flavonoids and vitamin E on cyclooxygenase-2 (COX-2) transcription***. Mutat Res., 2004. **551**: p. 245-254.

7. J.C. Le Bail, L.A., G. Habrioux ***Effects of pinostrobin on estrogen metabolism and estrogen receptor transactivation*** Cancer Letters, 2000. **156**: p. 37-44.

8. S. Tewtrakul, S.S., J. Puripattanavong, T. Panphadung, ***HIV-1 protease inhibitory substances from rhizomes of Boesenbergia pandurate Holtt*** Songklanakarin J SciTechnol., 2003. **25**: p. 503-508.

9. Y.F. Xian, S.P.I., Z.X. Lin, Q.Q. Mao, Z.R. Su, X.P. Lai *Protective effects of pinostrobin on β-amyloid-induced neurotoxicity in PC12 cell* Cell Mol Neurobiol., 2012. **32**: p. 1223-1230

10. N. Wu, Y.K., Y. Zu, Y. Fu, Z. Liu, R. Meng, X. Liu, T. Efferth, ***Activity investigation of pinostrobin towards herpes simplex virus-1 as determined by atomic force microscopy*** Phytomedicine., 2011. **18**: p. 110-118.

11. S. Atun, R.A., E. Sulistyowati, N. Aznam ***Isolation and antimutagenic activity of some flavanone compounds from Kaempferia rotunda*** Int J Chem Anal Sci., 2003. **4**: p. 3-8.

12. Geibel, M., ***Sensitivity of the fungus Cytospora persoonii to the flavonoids of Prunus cerasus*** Phytochemistry., 1995. **38**: p. 599-601

13. K. Kaur, M.J., T. Kaur, R. Jain ***Antimalarials from nature*** Bioorg Med Chem., 2009. **17**: p. 3229-3256.

14. SI. Abdelwahab, S.M., MA. Abdulla, MA. Sukari, AB. Abdul, MME. Taha, S. Syam, S. Ahmad, KH. Lee, ***The methanolic extract of Boesenbergia rotunda (L.) Mansf. and its major compound pinostrobin induces anti-ulcerogenic property in vivo: Possible involvement of indirect antioxidant action*** J Ethnopharmacol., 2011. **137**: p. 963- 970

15. N. Wu, K.F., YJ. Fu, YG. Zu, FR. Chang, YH. Chen, XL Liu, Y. Kong, W. Liu, CB. Gu ***Antioxidant Activities of Extracts and Main Components of Pigeonpea [Cajanus cajan (L.) Millsp.] Leaves*** Molecules, 2009. **14**: p. 1032-1043.

16. NK. Patel, K.B., ***Pinostrobin and Cajanus lactone isolated from Cajanus cajan (L.) leaves inhibits TNF-α and IL-1β production: in vitro and in vivo experimentation*** Phytomedicine., 2014. **21**: p. 946-953

17. JCL. Bail, L.A., G. Habrioux ***Effects of pinostrobin on estrogen metabolism and estrogen receptor transactivation*** Cancer Lett., 2000. **156**: p. 37-44

18. XD. Cao, Z.D., FS. Jiang, XH. Ding, JZ. Chen, SH. Chen, GY. Lv, ***Antitumor constituents from the leaves of Carya cathayensis*** Nat Prod Res., 2012. **26**: p. 2089-2094.

19. S. Charumanee, A.T., J. Sirithunyalug, P. Weiss-Greiler, P. Wolschann, H. Viernstein, S.Okonogi ***Thermodynamics of the encapsulation by cyclodextrins*** J Chem Technol Biotechnol, 2006. **81**: p. 523-529.

20. A. Ribeiro, A.F., D. Santos, F. Veiga, ***Preparation and solid-state characterization of inclusion complexes formed between miconazole and methyl-β-cyclodextrin***. AAPS Pharm Sci Tech., 2008. **9**: p. 1102-1109

21. J.L. Atwood, J.E.D.D., D.D. MacNicol, F. Vögtle In: J. Szejtli, T. Osa (ed) ***Comprehensive supramolecular chemistry***. Cyclodextrins, 3^{rd} edn, Pergamon, New York 1990.

22. A.L. Laza-Knoerr, R.G., P. Couvreur ***Cyclodextrins for drug delivery*** J. Drug Target, 2010. **18**: p. 645-656.

23. G. Tiwari, R.T., A. Rai ***Cyclodextrins in delivery systems: Applications*** J. Pharm Bioallied Sci, 2010. **2**: p. 72-79

24. A.E. Radi, S.E., ***Electrochemistry of cyclodextrin inclusion complexes of pharmaceutical compounds***. J. Open Chem Biomed Meth, 2010. **3**: p. 74-85.

25. C. Dass, W.J., ***Apolipoprotein A-I, cyclodextrins and liposomes as potential drugs for the reversal of atherosclerosis*** J. Pharm Pharmacol, 2000. **52**: p. 731-761.

26. Valle, E.M.M.D., ***Cyclodextrins and their uses: a review*** Process Biochem, 2004. **39**: p. 1033-1046

27. J. Wang, Z.C., ***Investigation of inclusion complex of miconazole nitrate with β-cyclodextrin*** Carbohydr Polym., 2008. **72**: p. 255-260

28. Ueno, A., ***Review: Fluorescent cyclodextrins for molecule sensing*** Supramol. Sci., 1996. **3**: p. 31-36

29. L.J. Yang, S.X.M., S.Y. Zhou, W. Chen, M.W. Yuan, Y.Q. Yin, X.D. Yang ***Preparation and characterization of inclusion complexes of naringenin with β-cyclodextrin or its derivative*** Carbohydr Polym, 2013. **98**: p. 861-869.

30. L. Szente, J.S., ***Highly soluble cyclodextrin derivatives: chemistry, properties, and trends in development*** Adv Drug Deliv Rev, 1999. **36**: p. 17-28.

31. D.W. Frank, J.E.G.a.R.N.W., ***Cyclodextrin nephrosis in the rat*** Am J Pathol 1976. **83**: p. 367-382.

32. J. Miranda, T.M., F. Veiga, H. Ferraz ***Cyclodextrins and ternary complexes: technology to improve solubility of poorly soluble drugs*** Braz J Pharm Sci, 2011. **47**: p. 665-681

33. T. Loftsson, M.M., ***Cyclodextrins in topical drug formulations: theory and practice*** Int J Pharm, 2001. **225**: p. 15-30

34. C. Rajeswari, A.A., A. Javed, R.K. Khar, ***Cyclodextrins in drug delivery: An updated review*** AAPS Pharm Sci Tech 2005. **6**: p. E329-E357.

35. Szejtli, J., ***The properties and potential uses of cyclodextrin derivatives*** J. Inclusion Phenom Mol Recognit Chem, 1992. **14**: p. 25-36

36. R.L. Carrier, L.A.M., I. Ahmed ***The utility of cyclodextrins for enhancing oral bioavailability*** J. Controlled Release, 2007. **123**: p. 78-99.

37. S. Tommasini, D.R., R. Ficarra, M.L. Calabrò, R. Stancanelli, P. Ficarra ***Improvement in solubility and dissolution rate of flavonoids by complexation with β-cyclodextrin***. J Pharm Biomed Anal, 2004. **35**: p. 379-387.

38. C. Jullian, L.M., C. Yañez, C. Olea-Azar, ***Complexation of quercetin with three kinds of cyclodextrins: An antioxidant study*** Spectrochem Acta Part A, 2007. **67**: p. 230-234.

39. R. Chadhaa, S.G., G. Shukla, D.V.S. Jain, R. R.S. Pissurlenkar, E.C. Coutinho ***Interaction of artesunate with β-cyclodextrin : Characterization, thermodynamic parameters, molecular modeling, effect of PEG on complexation and antimalarial activity*** Results Pharma Sci, 2011. **1**: p. 38-48

40. A. Semalty, Y.T., M. Semalty ***Preparation and characterization of cyclodextrin inclusion complex of naringenin and critical comparison with***

phospholipid complexation for improving solubility and dissolution J Therm Anal Calorim, 2014. **115**: p. 2471-2478.

41. S. K. Upadhyay, S.M.A., ***Solution structure of loperamide and β-cyclodextrin inclusion complexes using NMR spectroscopy*** J Chem Sci., 2009. **121**: p. 521-527

42. CM. Hsu, S.Y., FJ. Tsai, Y. Tsai ***Enhancement of rhubarb extract solubility and bioactivity by 2-hydroxypropyl-β-cyclodextrin*** Carbohydr Polym, 2013. **98**: p. 1422-1429.

43. T.A. Nguyen, B.L., J. Zhao, D. Thomas, J. Hook, ***An investigation into the supramolecular structure, solubility, stability and antioxidant activity of rutin/cyclodextrin inclusion complex***. Food Chem, 2013. **136**: p. 186-192

44. ZE. Pápaya, Z.S., K. Ludányia, N. Kállaia, E. Balogha,A. Kósab, S. Somavarapuc, B. Böddib, I. Antala ***Comparative evaluation of the effect of cyclodextrins and pH onaqueous solubility of apigenin*** J. Pharm. Biomed. Anal, 2016. **117**: p. 210-216.

45. A. García, D.L., M. O. Salazar, M. C. Lamas ***Modified β-Cyclodextrin Inclusion Complex to Improve the Physicochemical Properties of Albendazole. Complete In Vitro Evaluation and Characterization*** PLoS ONE, 2014. **9**.

46. H. Zhang, W.F., C. Li, T. Tan ***Investigation of the inclusions of puerarin and daidzin with β-cyclodextrin by molecular dynamics simulation*** J Phy Chem, 2010. **114**: p. 4876-4883.

47. Y. Zheng, C., H.L. Albert, Haworth, S. Ian, ***Molecular modeling of flavonoid-β-cyclodextrin complexes***. Lett Drug Des Discov 2008. **5**: p. 512-520.

48. B. Nutho, W.K., C. Rungnim, P. Pongsawasdi, P. Wolschann, A. Karpfen, N. Kungwan, T. Rungrotmongkol ***Binding mode and free energy prediction of fisetin/β-cyclodextrin inclusion complexes*** Beilstein J Org Chem, 2014. **10**: p. 2789-2799.

49. W. Sangpheak, W.K., P. Wolschann, P. Pongsawasdi, T. Rungrotmongkol ***Enhanced stability of a naringenin/2,6-dimethyl β-cyclodextrin inclusion complex: molecular dynamics and free energy calculations based on MM- and QM-PBSA/GBSA*** J Mol Graph Model, 2014. **50**: p. 10-15.

50. H. Zhang, T.T., C. Hetényi, D. Spoel, ***Quantification of solvent contribution to the stability of noncovalent complexes*** J. Chem. Theory Comput, 2013. **9**: p. 4542−4551.

51. W. Snor, E.L., P. Weiss-Greiler, A. Karpfen, H. Viernstein, P. Wolschann ***On the structure of anhydrous β-cyclodextrin***. Chem Phys Lett, 2007. **441**: p. 159-162.

52. I. Alecu, J.Z., Y. Zhao, D.G. Truhlar ***Computational Thermochemistry: Scale factor database and scale factors of vibrational frequencies obtained from electronic model chemistries*** J Chem Theory Comput, 2010. **6**: p. 2872-2887

53. R.C. Walker, M.F.C., D.A. Case ***The Implementation of a fast and accurate QM/MM potential method in AMBER*** J Comp Chem, 2008. **29**: p. 1019-1031

54. K.N. Kirschner, A.B.Y., S.M. Tschampel, J. Gonzalez-Outeirino, C.R. Daniels, B.L. Foley, R.J. Woods, ***GLYCAM06: A generalizable biomolecular force field carbohydrates*** J Comp Chem, 2008. **29**: p. 622-655.

55. W. Khuntwee, T.R., S. Hannongbua ***Molecular dynamic behavior and binding affinity of flavonoid analogues to the cyclin dependent Kinase 6/cyclin D complex*** J Chem Inf Mol, 2012. **52**: p. 76-83.

56. N. Kaiyawet, T.R., S. Hannongbua ***Effect of halogen substitutions on dUMP to stability of thymidylate synthase/dUMP/mTHF ternary complex using molecular dynamics simulation*** J Chem Inf Model, 2013. **6**: p. 1315-1323.

57. A. Meeprasert, T.R., M.S. Li, S. Hannongbua ***In silico screening for potent inhibitors against the NS3/4A protease of hepatitis C virus***. Curr Pharm Des, 2014. **20**: p. 3465-3477.

58. A. Meeprasert, W.K., K. Kamlungsua, N. Nunthaboot, T. Rungrotmongkol, S. Hannongbua ***Binding pattern of the long acting neuraminidase inhibitor laninamivi towards influenza A subtypes H5N1 and pandemic H1N1***. J Mol Graphics Model, 2012. **38**: p. 148-154.

59. A. Meeprasert, S.H., T. Rungrotmongkol ***Binding and susceptibility of NS3/4A serine protease inhibitors against hepatitis C virus***. J Chem Inf Model, 2014. **54**: p. 1208-1217

60. B.A. Luty, W.F.G., ***Calculating electrostatic interactions using the particle-particle particle-mesh method with nonperiodic long-range interactions*** J Phys Chem, 1996. **100**: p. 2581-2587.

61. A. Silva, W.V., ***ACPYPE - AnteChamber PYthon Parser interfacE*** BioMed Central, 2012. **5**: p. 1-8.

62. T. Higuchi, K.A.C., ***Phase solubility techniques*** Adv Anal Chem Instrum, 1965. **4**: p. 117-122.

63. A. Bax, D.G.D., ***Practical aspects of two-dimensional transverse NOE spectroscopy***. J. Magn. Reson, 1985. **63**: p. 207-213

64. T.L. Hwang , A.J.S., ***Cross relaxation without TOCSY: transverse rotating-frame Overhauser effect spectroscopy*** J. Am. Chem. Soc, 1992. **114**: p. 3157-3159.

65. M. Mueller, S.H., A. Jungbauer, ***Anti-inflammatory activity of extracts from fruits, herbs and spices***. Food Chem, 2010. **122**: p. 987-996.

66. W. Sangpheak, J.K., R. Schuster, T. Rungrotmongkol, P. Wolschann, N. Kungwan, H. Viernstein, M. Mueller and P. Pongsawasdi ***Physical properties and biological activities of hesperetin and naringenin in complex with methylated β-cyclodextrin*** Beilstein J. Org. Chem, 2015. **11**: p. 2763-2773.

67. C.W. Yong, C.W., W. Smith, ***Structural Behaviour of 2-Hydroxypropyl-β-Cyclodextrin in Water: Molecular Dynamics Simulation Studies*** Pharm Res, 2007. **25**: p. 1092-1099.

68. T. Kozar, C.V., ***Reconsidering the conformational flexibility of β-cyclodextrin*** Thermochem, 1997. **395-396** p. 451-468.

69. P. Greenidge, C.K., J.C. Mozziconacci, R. Wolf ***MM/GBSA binding energy prediction on the PDBbind data set: successes, failures, and directions for further improvement*** J Chem Inf Model, 2013. **53**: p. 201-209.

70. V. Zoete, M.M., M. Karplus ***Study of insulin dimerization: binding free energy calculations and per-residue free energy decomposition*** Proteins: structure, function, and bioinformatics, 2005. **61**: p. 79-93.

71. S. Genheden, O.K., P. Mikulskis, D. Hoffmann, U. Ryde ***The normal-mode entropy in the MM/GBSA method: effect of system truncation, buffer region, and dielectric constant*** J Chem Inf Model, 2012. **52**: p. 2079-2088.

72. S.K. Ludemann, V.L., R. C. Wade ***How do substrates enter and products exit the buried active site of cytochrome P450 cam?*** . J. Mol. Biol, 2000. **303**: p. 813-830.

73. D. Zhang, J.G., J.A. McCammon ***Potentials of mean force for acetylcholine unbinding from the alpha7 nicotinic acetylcholine receptor ligand-binding domain*** J. Am. Chem. Soc, 2006. **128**: p. 3019–3026.

74. F. Colizzi, R.P., L. Scapozza, M. Recanatini, A. Cavalli ***Single-molecule pulling simulations can discern active from inactive enzyme inhibitors*** J. AM. CHEM. SOC., 2010. **132**: p. 7361-7371.

75. J. Caballero, C.Z., D. Aguayo, C. Yanez, FD. Gonza´lez-Nilo ***Study of the interaction between progesterone and β-cyclodextrin by electrochemical techniques and steered molecular dynamics*** J. Phys. Chem. B., 2008. **112**: p. 10194-10201.

76. N. Rawashdeh, K.A.-S., M. Al-Bitar ***Inclusion Complexes of Sunscreen Agents with β-Cyclodextrin: Spectroscopic and Molecular Modeling Studies*** J. Spectrosc 2013. **11**: p. 1-11.

77. R. Chadha, S.G., G. Shukla, D.V.S. Jain, R. Pissurlenkar, E. Coutinho ***Interaction of artesunate with β-cyclodextrin: Characterization, thermodynamic parameters, molecular modeling, effect of PEG on complexation and antimalarial activity*** Results Pharma Sci, 2011. **1**: p. 38-48.

78. J. W. Wong, K.H.Y., ***Inclusion Complexation of Artemisinin with α-, β-, and γ-Cyclodextrins*** Drug Dev Ind Pharm, 2003. **29**: p. 1035-1044

79. B. Liu, W.L., J. Zhao, Y. Liu, X. Zhu, G. Liang ***Physicochemical characterisation of the supramolecular structure of luteolin/cyclodextrin inclusion complex*** Food Chem, 2013. **141**: p. 900-906.

80. N. Rajendiran, S.S., ***Inclusion complex of sulfadimethoxine with cyclodextrins: Preparation and characterization***. Carbohydr Polym, 2014. **101**: p. 828-836.

81. DW. Wang, C.O., Q. Liu, HL. Yuan, XH. Liu ***Inclusion of quinestrol and 2,6-di-O-methyl-β-cyclodextrin: Preparation, characterization, and inclusion mode*** Carbohydr Polym, 2013. **93**: p. 753-760.

82. C. Folch-Cano, J.G., H. Speisky, C. Jullian, C. Olea-Azar ***NMR and molecular fluorescence spectroscopic study of the structure and thermodynamic parameters of EGCG/ b-cyclodextrin inclusion complexes with potential antioxidant activity*** J Incl Phenom Macrocycl Chem, 2014. **78**: p. 287-298.

83. Y. Yao, Y.X., C. Hong, G. Lic, H. Shenb, G. Jia, ***Development of a myricetin/hydroxypropyl-β-cyclodextrin inclusion complex: Preparation, characterization, and evaluation*** Carbohydr Polym, 2014. **110**: p. 329-337.

84. A. Semalty, Y.T., M. Semalty ***Preparation and characterization of cyclodextrin inclusion complex of naringenin and critical comparison with phospholipid complexation for improving solubility and dissolution***. J Therm Anal Calorim., 2014. **115**: p. 2471-2478

85. C. Wagner, E.J., F. Kesisoglou, M. Vertzoni, C. Reppas, JB. Dressman ***Predicting the oral absorption of a poorly soluble, poorly permeable weak base using biorelevant dissolution and transfer model tests coupled with a physiologically based pharmacokinetic model*** Eur J Pharm Biopharm, 2012. **82**: p. 127-138.

86. R. Bikádi, S.K., J.S. Balogh, E.H. zeman ***Aggregation of cyclodextrins as an important factor to determine their complexation behavior***. Chem. Biodivers, 2006. **3**: p. 1266-1278.

87. A. Zhang, W.L., L. Wang, Y. Wen ***Characterization of inclusion complexation between fenoxaprop-p-ethyl and cyclodextrin*** J. Agric. Food Chem, 2005. **53**: p. 7193-7197.

88. Á. Nacsa, O.B., P. Szabó-Révész, Z. Aigner ***Achievement of pH-independence of poorly-soluble: ionizable loratadine by inclusion complex formation with dimethyl-β-cyclodextrin*** J. Incl. Phenom. Macrocyclic Chem, 2009. **64**: p. 249-254.

89. SI. Abdelwahab, S.M., MA. Abdulla, MA. Sukari, AB. Abdul, MME. Taha, S. Syam, S. Ahmad, KH. Lee ***The methanolic extract of Boesenbergia rotunda (L.) Mansf. and its major compound pinostrobin induces anti-ulcerogenic property in vivo: Possible involvement of indirect antioxidant action***. J Ethnopharmacol, 2011. **137**: p. 963- 970.

90. J.S. Ashidi, P.J.H., P.J. Hylands, T. Efferth, ***Ethnobotanical survey and cytotoxicity testing of plants of South-western Nigeria used to treat cancer, with isolation of cytotoxic constituents from Cajanus cajan Millsp. Leaves***. J Ethnopharmacol, 2010. **128**: p. 501-512.

91. N.M. Isa, S.I.A., S. Mohan, A.B. Abdul, M.A. Sukari, M.M.E. Taha, S. Syam, P. Narrima, S.Ch. Cheah, S. Ahmad, M.R. Mustafa ***In vitro anti-inflammatory, cytotoxic and antioxidant activities of boesenbergin A, a chalcone isolated from Boesenbergia rotunda (L.) (fingerroot)***. Braz. J. Med. Biol. Res, 2012. **45**: p. 524-530.

92. H.D. Smolarz, E.M., A. Bogucka-Kocka, J. Kocki, ***Pinostrobin - an anti-leukemic flavonoid from Polygonum lapathifolium L. ssp. nodosum (Pers.) Dans*** Z. Naturforsch. C Bio. Sci, 2006. **61**: p. 64-68.

APPENDIX

VITA

Miss Jintawee Kicuntod, 3rd year M.Sc. student

Current institution & address:

Biochemistry, Science, Chulalongkorn University, 254 Phayathai Road, Bangkok 10330, Thailand

Academic information:

2013-Present M.Sc. student Biochemistry and molecular biology, Chulalongkorn University

2009-2012 B.Sc. (2nd Class Honours) Biochemistry, Chulalongkorn University

Master's degree scholarship (present):

The 72nd Anniversity of His Majesty King Bhumibala Aduladeja, Chulalongkorn University

The 90th Anniversary of Chulalongkorn University Fund (Ratchadaphiseksomphot Endowment Fund)